Molecular Hydrogen Attenuated N-methyl-N-Nitrosourea Induced Corneal Endothelial Injury by Upregulating Anti-Apoptotic Pathway

Runpu Li,[1,2] Yingxin Qu,[3] Xiaoqi Li,[1,2] Ye Tao,[4] Qinghua Yang,[2] Junyi Wang,[2] Yumei Diao,[2] Qian Li,[2] Yifan Fang,[1,2] Yifei Huang,[2] and Liqiang Wang[2]

[1]Medical School of Chinese PLA, Beijing, China
[2]Department of Ophthalmology, The Third Medical Center, Chinese PLA General Hospital, Beijing, China
[3]Department of Ophthalmology, Chinese Aerospace 731 Hospital, Beijing, China
[4]Department of Ophthalmology, Henan Provincial People's Hospital, Zhengzhou University, Zhengzhou, China

PURPOSE. Previous work by our group has demonstrated the value of N-methyl-N-nitrosourea (MNU)-induced corneal endothelial decompensation in animal models. The aim of this study was to investigate the effect of molecular hydrogen (H_2) on MNU-induced corneal endothelial cell (CEC) injury and the underlying mechanism.

METHODS. MNU-induced animal models of CEC injury were washed with hydrogen-rich saline (HRS) for 14 days. Immunofluorescence staining, immunohistochemical staining, and corneal endothelial assessment were applied to determine architectural and cellular changes on the corneal endothelium following HRS treatment. MNU-induced cell models of CEC injury were co-cultured with H_2. The effect of H_2 was examined using morphological and functional assays.

RESULTS. It was shown that MNU could inhibit the proliferation and specific physiological functions of CECs by increasing apoptosis and decreasing the expression of ZO-1 and Na^+/K^+-ATPase, whereas H_2 improved the proliferation and physiological function of CECs by anti-apoptosis. Cell experiments further confirmed that H_2 could reverse MNU damage to CECs by decreasing oxidative stress injury, interfering with the NF-κB/NLRP3 pathway and the FOXO3a/p53/p21 pathway.

CONCLUSIONS. This study suggests that topical application of H_2 could protect CECs against corneal damage factors through anti-apoptotic effect, reduce the incidence and severity of corneal endothelial decompensation, and maintain corneal transparency.

Keywords: anti-apoptotic effect, corneal endothelial decompensation, molecular hydrogen, N-methyl-N-nitrosourea

Corneal endothelial cells (CECs), which are closely connected to each other, are monolayer cells located in the innermost layer of the cornea. By regulating nutrition and hydration, CECs play a decisive role in maintaining corneal function.[1] From 5 to 6 weeks of fetal development, human corneal endothelial cells (HCECs) have been blocked in the G1 phase of the cell cycle and basically lose the opportunity for endogenous replenishment.[2,3] Inflammation, trauma, or immune response can cause irreversible damage to CECs, leading to corneal endothelial decompensation, one of the most serious and intractable diseases that can lead to blindness.[4] Fuchs endothelial corneal dystrophy (FECD) is the most common cause of corneal endothelial decompensation worldwide.[5] In addition, phacoemulsification is also a common cause of corneal endothelial damage.[6] At present, the main treatment for corneal endothelial decompensation is corneal endothelium transplantation. In the United States, 56% of corneal transplants are associated with vision loss related to endothelium depletion.[7] However, there are problems in clinical practice, such as insufficient number of donated corneas and severe graft reaction.[8,9] Many relevant therapeutic studies are under way, but none of them has been widely used in clinical practice until now.[10] One of the research bottlenecks is that there is no suitable animal model of corneal endothelial decompensation. Previously, our team has constructed an N-methyl-N-nitrosourea (MNU)-induced corneal endothelial decompensation model.[11]

MNU is represented by the molecular formula $C_2H_5N_3O_2$. As an alkylating agent that directly acts on DNA, it is widely believed that it can induce apoptosis of cells,[12–14] including eye cells.[15,16] Hayakawa and coworkers have shown that MNU can affect a variety of eye cells, resulting in continuous ultrastructural changes.[17] With significant corneal edema in a dose- and time-dependent way, our model could simulate the natural process of corneal endothelial injury to a certain extent.

Based on the mature rabbit corneal endothelial decompensation model, this study attempted to explore the protective effect of hydrogen molecule (H$_2$) on the endothelium of the model and its mechanism. H$_2$, a colorless and odorless small gas molecule, can quickly and effectively penetrate biological membranes to reach the cytoplasm, nucleus, and mitochondria, and the blood-brain barrier and blood-eye barrier cannot block H$_2$.[18,19] Low concentration of H$_2$ has been regarded as an effective reducing agent with little side effects, and has become a new type of medical gas that has attracted wide attention in recent years. The safety of H$_2$ is characterized by excellent histocompatibility and extremely low cytotoxicity, even at high concentrations.[20] H$_2$ has significant preventive and therapeutic effects on the pathological states of various organs, and its protective mechanisms are related to antioxidant, anti-inflammatory, and anti-apoptotic functions.[18,19,21–24] The realization of these effects involves multiple signaling pathways and crosstalk, and the pluripotency of H$_2$ on various proteins, molecules, and signaling pathways may at least partially explain its pluripotent therapeutic potential.[23] Compared with other diseases, the research on the relationship between H$_2$ and corneal diseases is still in the initial stage. Only one study proved that the alkali injury of rabbit cornea could be reversed by washing with H$_2$ solution immediately after injury.[25]

In this study, the MNU-induced CEC injury animal model and cell model were adopted to explore the anti-apoptotic effect, the molecular mechanism and targets of H$_2$ on CECs in vivo and in vitro. It provides an effective method and theoretical basis for the clinical application of hydrogen-rich saline (HRS).

## MATERIALS AND METHODS

Animal

All of the experiments complied with the ARVO Statement for the Use of Animals in Ophthalmic and Vision Research. All operations and treatments related to laboratory animals have been approved by the Institutional Animal Care and Use Committee of the General Hospital of Chinese PLA. Adult New Zealand rabbits (male rats, approximately 2.0–2.5 kg, 12 months old) were purchased from Beijing Jinmuyang Laboratory Animal Breeding Co, Ltd., and raised under SPF1 conditions. Animal experiments were conducted after rabbits were fed for 1 week.

Cell Culture

The immortalized CEC line B4G12 was purchased from Creative Bioarray (Shirley, NY, USA) and cultured in human endothelial serum-free medium (SFM; Creative Bioarray) containing 3% fetal bovine serum (FBS) and 1% penicillin and streptomycin.[26] The cells were incubated with 6 and 96-well plates in an MCO-20AIC cell incubator (Panasonic, Japan) at 25°C and 5% CO$_2$.

Storage and Use of MNU

MNU (Fluorochem Ltd, UK) was stored at −20°C under dark conditions.[27] A corneal endothelial decompensation animal model was constructed based on our previous method: any rabbit eye was selected and a 150 μL mixture of 30% dimethyl sulfoxide (DMSO; SERVA, Heidelberg, Germany) and 70% PBS with 3.0 mg/kg body weight of MNU was
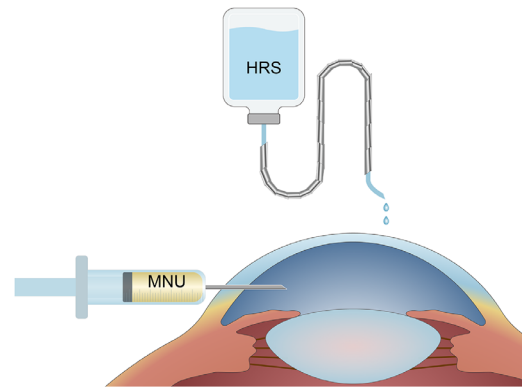
FIGURE 1. Schematic diagram of animal operation. A 150 μL mixture of 30% DMSO and 70% PBS with 3.0 mg/kg body weight of MNU was injected into the anterior chamber of rabbits through the corneal limbus with a sterile 30-gauge steel needle. Within 1 week before and after injection of MNU, rabbit eyes were irrigated with HRS 3 times a day for 3 minutes and 3 drops per second, whereas the control eyes were irrigated with saline ($n = 8$).

injected into the anterior chamber through the corneal limbus with a sterile 30-gauge steel needle, whereas the other eye was not operated on, in order to serve as a normal control and not excessively reduce the quality of life of New Zealand rabbits (Fig. 1).[11,28] The CEC injury model was constructed by dissolving MNU with phosphate buffered saline (PBS) in the dark to make it an MNU solution with a concentration of 80 mmol/L, adding MNU solution into the culture medium containing cells that had been starved for 24 hours, and diluting MNU to a concentration of 6 mmol/L.

Preparation and Application of H$_2$

The SFH-300 hydrogen generator (Bangyes, Shanghai, China) was used to produce H$_2$. The H$_2$ was pumped through a sealed pipeline into a 100 mL saline bottle (Qidu Pharmaceutical Co., Ltd., Shandong, China) containing saline or culture medium and pressurized to 0.4 MPA. The saline bottle was sealed with sealing film, fully wrapped with tin foil, and placed at 4°C for 24 hours before use. The whole process of the operation was carried out under aseptic conditions and was freshly prepared by the same experimental operator before each use.[27] Within 1 week before and after injection of MNU, rabbit eyes were irrigated with HRS 3 times a day for 3 minutes and 3 drops per second, whereas the control eyes were irrigated with saline or not irrigated ($n = 8$; see Fig. 1). When the CECs were interfered, the medium containing H$_2$ was replaced simultaneously with 6 mmol/L MNU. The mass ratio of H$_2$ in solution, determined using DH200 Hydrogen Concentration Detector (CLEAN, Shanghai, China), is maintained above 1.2 ppm.

Anterior Segment Examination of Rabbit Eyes

After MNU was injected into the anterior chamber, slit lamp photography (Opto-sil, Optoprobe, UK) and anterior segment optical coherence tomography (AS-OCT; Visante OCT 1000; Carl Zeiss) were performed to examine rabbit eyes at day 1, day 3, day 7, day 14, day 21, and day 28, respectively. Slit lamp microscope was used to observe the anterior segment. AS-OCT was used to measure the central corneal

thickness (CCT) and the average value of three measurements was recorded.

Immunofluorescence Staining of Rabbit Corneas

The corneal specimens were embedded in optimal cutting temperature) compound (SAKURA, Japan). The corneas were cut into 6 µm thick sections in sagittal plane with Cryotome E cryostat (Thermo Fisher Scientific, Waltham, MA, USA). The sections were placed on coverslips coated with polylysine for immunofluorescence staining. The tissue sections were fixed, washed, and repaired with pH 6.0 citric acid repair solution (Servicebio, Wuhan, China). The BSA serum was added for 30 minutes. The coverslips were incubated with the primary antibody (anti-α 1 Na$^+$/K$^+$-ATPase antibody, Abcam, ab7671, 1:200) at 4°C overnight, washed with PBS, and incubated with the secondary antibody connected to the fluorophore (Cy3 labeled goat anti-mouse; Servicebio; GB21301, 1:100) for 50 minutes to demonstrate the immunoreactivity. After DAPI re-staining the nucleus, anti-fade mounting medium was used to block the coverslips.

TUNEL Staining of Rabbit Corneas

After rewarming and drying, the frozen sections of corneal tissue were fixed with cold acetone (Sinopharm, China) for 10 minutes, then washed with PBS. The coverslips were incubated with protease K working solution (Servicebio) in the incubator for 37 minutes and covered with permeabilize working solution for 20 minutes after rinsed. TdT and dUTP were mixed (ratio 1:9) according to the instruction of TUNEL kit (Roche, Switzerland), used to cover the tissue, and incubated at constant temperature for 2 hours. After DAPI re-staining the nucleus, anti-fade mounting medium was used to block the coverslips.

Reactive Oxygen Species Staining of Rabbit Corneas

Liquid blocker pen (Gene Tech, USA) was used to draw a circle around the tissue on the frozen section to prevent the liquid from slipping away. Dihydroethidium (DHE; Sigma-Aldrich; D7008, 1:500) dripped in the circle and was incubated at 37°C without light for 30 minutes. After DAPI re-staining the nucleus, anti-fade mounting medium was used to block the coverslips. The results of immunofluorescence staining, TUNEL staining, and reactive oxygen species (ROS) staining of rabbit corneas were visualized using Nikon Eclipse C1 positive fluorescence microscope and Nikon DS-U3 imaging system. The average fluorescence intensity was measured by Image J software, and the results were semi-quantitatively analyzed.

Immunohistochemical Staining of Rabbit Corneas

The corneal paraffin sections were deparaffinized and rehydrated for antigen retrieval. Serum was used to block the activity of endogenous peroxidase. The coverslips were incubated overnight at 4°C, together with the primary antibody (8-OHdG; Abcam; ab48508, 1:100), washed with PBS (pH 7.4, for 5 minutes) for 3 times and then incubated with the secondary antibody (goat anti-mouse antibody; Servicebio; GB23301, 1:200) at room temperature for 50 minutes. Freshly prepared DAB chromogenic reagent (Servicebio; G1211) was used to mark dried coverslips. The reaction time was determined by microscope observation, and the qualified mark was brown-yellow nucleus. The coverslips were washed with distilled water (5 minutes each). The color digital images of hematoxylin and eosin (H&E) staining and 8-hydroxy-2-deoxyguanosine (8-OHdG) immunohistochemical staining were obtained from a high-resolution digital coverslip scanner (NanoZomer 2.0 digital coverslip scanners; Hamamatsu subsidiary, Bimatsu, Japan). The average gray values of 8-OHdG immunohistochemical staining images were measured by Image J software.

In vivo Confocal Microscope of Rabbit Corneas

At day 1, day 3, day 7, day 14, day 21, and day 28, an in vivo confocal microscope (IVCM; HRT III; Heidelberg Engineering, Germany, Heidelberg Engineering) was used to observe the rabbit cornea. Fifty to 100 IVCM images parallel to corneal epithelium, stroma, and endothelium were obtained.

Electron Microscopy Scanning of Rabbit Corneas

The corneal specimens obtained were examined by electron microscopy. First, the corneal specimens were immersed in a stationary liquid of 0.1 M sodium bicarbonate (pH 7.4; Electron Microscopy Science, Hatfield, PA, USA) containing 2.5% glutaraldehyde overnight at 4°C. Then, the corneal specimens were immersed in 1% osmium tetroxide (FMB, Singapore) at 22°C for 2 hours. Next, the corneal specimens were dehydrated in a series of ethanol diluents, dried in a critical point dryer (BALTEC, Balzers, Liechtenstein), and installed on a holder. At last, a 10 nm thick gold layer of (BALTEC) was sputtered on the specimens that were examined by scanning electron microscope (SEM; FEI, Holland).

Histological Analysis of Rabbit Corneal Sections

The experimental animals were euthanized with excess pentobarbital sodium (Beijing Huaye Huayu Chemical Co., Ltd., China) at day 1, day 3, day 7, day 14, day 21, and day 28, respectively. The corneas were taken for subsequent examination. Part of the corneal specimen was placed on the coverslip (endothelium facing up), smeared with 0.25% trypan blue for 1 minute, alizarin red S (1% pH 4.2) for 3 minutes, and then observed under an inverted optical microscope (BX51; Olympus, Japan). Ten percent of neutral buffer formalin was used to fix the other part of the corneal specimen, which were then processed into 4 µm thick paraffin sections for H&E staining and immunohistochemical staining.

Image Acquiring of CECs

CECs were cultured on 6-well plates. When the adherent cells grew to 70%, they were starved for 24 hours and then divided into 4 groups (the control group, MNU group, H₂ group, and MNU + H₂ group). Medium containing MNU and/or H₂ were replaced in all groups except the control group. ZOE Fluorescent Cell Imager (Bio-Rad, Hercules, CA, USA) was used at 6 hours and 24 hours after intervention.

Cell Counting Kit-8 Test of CECs

The medium containing H_2 and the blank medium were added into 96-well plates, respectively. The media were mixed with 10 µl cell counting kit 8 (CCK-8) solution (Dojindo, Japan) at different time points (2, 4, 6, 12, 24, 36, and 48 hours) and incubated for 2 hours. The absorbance at 450 nm was determined by Imark enzyme labeling instrument (Bio-Rad). The CECs were cultured in 96-well plates with cell suspension of 100 µL per well (about 5000 cells), divided into the control group, MNU group, HRS group, and MNU + HRS group. Finally, CCK-8 tests were performed under the same conditions at 2, 4, 6, 12, and 24 hours after intervention, and the cytotoxicity of MNU and the effect of H_2 on CECs were evaluated.

Immunofluorescence Staining of CECs

Coverslips were placed in the 6-well plates of cultured cells, collected when the cells grew to 70 to 90%. The coverslips were fixed by 4% paraformaldehyde (Servicebio) for 15 minutes, covered, and blocked with 3% bovine serum albumin (BSA; Servicebio) for 30 minutes at room temperature (if the primary antibody was from goat, 10% normal rabbit serum was used to block it), and then incubated with the primary antibody (ZO-1, Servicebio, GB111402, 1:800; Na^+/K^+-ATPase, Santa, sc-21712, 1:50; Bax, Abcam, ab32503, 1:200; Bcl-2, Abcam, ab182858, 1:200; caspase-3, Abcam, ab13847, 1:200; caspase-9, Abcam, ab202068, 1:200; NFκB p65, Servicebio, GB11142, 1:100; NLRP3, Servicebio, GB11300, 1:500; ASC, Proteintech Group, 40500-1-AP, 1:100; caspase-1, Boorsen, BS-10743R, 1:200; IL-1β, Servicebio, GB11113, 1:200; FoxO3a, CST, 2497, 1:200; p53, Gene Tex, GTX70214, 1:500; p21, Gene Tex, GTX629543, 1:200) overnight in a wet box at 4°C. The cell samples were covered with secondary antibodies of the corresponding species (Cy3 labeled goat anti-rabbit, Servicebio, GB21303, 1:300; Cy3 labeled goat anti-mouse, Servicebio, GB21301, 1:300), and incubated at room temperature for 50 minutes. The 4′,6-diamidino-2-phenylindole (DAPI; ServiceBio) was used to re-stain the nucleus and anti-fade mounting medium (Servicebio) was used to seal the coverslips.

TUNEL Staining of CECs

After fixed with 4% paraformaldehyde (Servicebio) for 15 minutes, the CEC-seeded coverslips was treated with membrane breaking solution (Servicebio) and permeabilize working solution (Servicebio). According to the instruction of TUNEL kit (Servicebio), TdT, dUTP, and buffer (ratio 1:5:50) were mixed and used to cover cells. After incubation at constant temperature for 2 hours, DAPI was used to re-stain the nucleus and anti-fade mounting medium was used to seal the coverslips. Immunofluorescence images and the TUNEL staining results of CECs were visualized using the Nikon Eclipse C1 positive fluorescence microscope (Nikon, Japan) and the Nikon DS-U3 imaging system (Nikon, Japan). Image J Software (National Institutes of Health [NIH], Bethesda, MD, USA) was used to measure the average fluorescence intensity and the results obtained were semiquantitatively analyzed.

Western Blotting Assay of CECs

The CECs were treated with radio immunoprecipitation assay (RIPA) lysis buffer (Servicebio), which was added with phosphorylated protease inhibitors (Servicebio) 5 minutes before, scraped off, collected, and centrifuged at 4°C for 10 minutes (12,000 rpm) using a D3024R high-speed refrigerated centrifuge (DragonLab, China). The supernatant was collected. The bicinchoninic acid (BCA) protein assay kit (Beyotime, Shanghai, China) was used to determine the protein concentration and then the protein was denatured. Sodium dodecyl sulphate polyacrylamide gel electrophoresis (SDS-PAGE; Servicebio) results were transferred to polyvinylidene difluoride (PVDF) membrane (Servicebio). The PVDF membrane was blocked with tris buffered saline Tween (TBST; Servicebio) and skim milk for 30 minutes and incubated with diluted primary antibodies (Bax, Abcam, ab32503; Bcl-2, Abcam, ab182858; caspase-3, Abcam, ab13847; caspase-9, Abcam, ab202068; NFκB p65 Servicebio, GB11142; FOXO3a, CST, 2497) at 4°C and slowly shaken overnight. The secondary antibody (HRP labeled goat anti-rabbit, Servicebio, GB23303; HRP labeled goat anti-mouse, Servicebio, GB23301) was diluted according to the ratio of 1: 5000 after the PVDF membrane being washed with TBST buffer for 3 times. After the secondary antibodies were washed off by TBST buffer, the strips were chemiluminescent with ECL solution (Servicebio), scanned by V370 scanner (Epson, Japan), decolorized by Photoshop software, and analyzed by Alpha software processing system.

## Reverse Transcription-Polymerase Chain Reaction Assay of CECs

The cells disrupted with RNA extraction solution (Servicebio), together with chloroform (Sinopharm, China), was centrifuged in a D3024R high-speed refrigerated centrifuge (DragonLab, China) at 4°C for 10 minutes (12,000 rpm). The RNA precipitation was obtained by centrifugation of extracted supernatant and 0.8 times the volume of isopropanol (Sinopharm, China), washed with 75% ethanol (Hyclone, USA), dissolved in RNA-free water, tested for concentration and purity using NanoDrop2000 Ultra-Microscale Spectrophotometer (Thermo, USA) and diluted to ensure that the concentration was between 100 ng/µL and 500 ng/µL. The reverse transcription reaction was performed using ServiceBio RT First Strand cDNA Synthesis Kit (Servicebio). The quantitative PCR reaction system was composed of reverse transcription products, $2 \times$ SYBR Green qPCR Master Mix (High Rox; ServiceBio) and gene primers. The results of PCR amplification were obtained using the $2^{-\Delta CT}$ method analysis.

Oxidative Stress Detection of CECs

The cells were cultured in 6-well plates. The protein was obtained by using cell lysis buffer for Western and IP (Beyotime, Shanghai, China). The protein concentration was determined by BCA protein assay kit (Beyotime). The Lipid Peroxidation Malondialdehyde Assay Kit (Beyotime), Total Glutathione Peroxidase Assay Kit (Beyotime), and Catalase Assay Kit (CAT; Beyotime) were used to analyze the CEC protein respectively. The absorbances of Malondialdehyde (MDA), glutathione (GSH), and catalase were measured at 532 nm, 340 nm, and 520 nm, respectively, by 722N spectrophotometer (Shanghai Scientific Instrument Co., Ltd., Shanghai, China).

Data Analysis and Statistics

All experiments were repeated three times independently. All data are presented as mean ± standard error of mean.
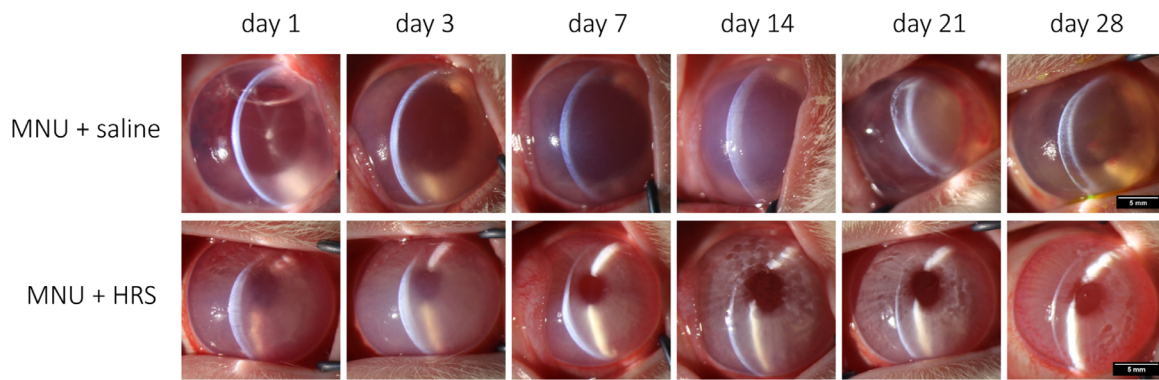
FIGURE 2. Slit-lamp microscopy examination of rabbit eyes. Inflammatory infiltration and irreversible corneal edema appeared in the rabbit eyes of the MNU + saline group from day 1 after intervention, and no corneal neovascularization was found. Rabbits in the MNU + HRS group showed significant corneal edema at day 1 and day 3 and corneal edema gradually decreased from day 7. Pupil size was maintained throughout. The corneas returned to normal at day 28. Magnification × 16. Scale bar = 5 mm.

Multiple *t*-test and 2-way ANOVA were used for group data, whereas single sample *t*-test and 1-way ANOVA were used for other data. All statistical calculations were performed by GraphPad Prism 8 software. $P < 0.05$ was considered statistically significant (*$P < 0.05$, **$P < 0.01$, ***$P < 0.001$, and ****$P < 0.0001$).

RESULTS

HRS Attenuated MNU-Induced Corneal Edema and Anterior Segmental Inflammation

During the 28 days from MNU intervention to euthanasia, the status of anterior segment of rabbits was observed. As shown in Figure 2, The corneal changes were identical in the rabbits irrigated with normal saline and those not irrigated. Slit lamp microscope was used to observe the anterior segment. Inflammatory infiltration, mydriasis similar to toxic anterior segment syndrome (TASS), and irreversible corneal edema appeared in the rabbit eyes of MNU + saline group from day 1 after intervention, and no corneal neovascularization was found.

Corneal edema was also seen in AS-OCT images (Fig. 3). However, the corneal injury was significantly alleviated in the MNU + HRS group, with smaller pupils and smaller CCT compared with the MNU + saline group ($P < 0.0001$, $n = 18$). There was no statistically significant difference in CCT between the MNU + saline group and the MNU + HRS group at day 1 and day 7, whereas there was statistically significant differences at day 3, day 14, day 21, and day 28 (day 1: $P = 0.5391$; day 3: $P < 0.05$; day 7: $P = 0.1569$; day 7: $P = 0.1569$; day 14: $P < 0.001$; day 21: $P < 0.0001$; and day 28: $P < 0.01$).

H&E staining of corneal sections showed that CECs in the MNU + saline group remained absent throughout the observation period, and Descemet's membrane (DM) layer damage was also observed in the MNU + saline group from day 14 after intervention. The CEC detachment in the MNU + HRS group was obvious from day 1 to day 7. Evidence of CEC regeneration was observed in the MNU + HRS group from day 14. The DM remained unaffected in the MNU + HRS group throughout the observation period. Changes in CCT corresponded with changes in CEC damage (Fig. 4).

HRS Attenuated MNU Induced CEC Injury

CECs of rabbits were further observed. Rabbit corneas were examined under IVCM. At day 1, sparse and blurred CECs could be seen in the MNU + saline group, and the CECs continued to decrease from day 3 to day 28. Correspondingly, the CECs in the MNU + HRS group were damaged at a slower speed from day 1 to day 7, showing high reflex, irregular and sparse CECs at day 7. In the MNU + HRS group, CECs regenerated from day 14 after intervention, and images of normal CECs were obtained at day 28, showing uniform hexagonal cells and low reflex on the edge, which meant a return to normal corneal endothelium (Fig. 5A).

SEM showed that a small number of deformed CECs or cellular residual structures could be seen at day 1 and day 3, CECs were rarely observed after day 7, and DM injury was observed after day 21 in the MNU + saline group. There were CEC deformation and structural disorder on the inner surface of the cornea in the MNU + HRS group at day 1 and day 3 and the regeneration of CECs after day 7, although the damage to the DM and CEC layer still existed (Fig. 5B).

The corneal specimens were stained with alizarin red S and trypan blue. It was found that intact cell structure became more difficult to observe in the MNU + saline group with time. In the MNU + HRS group, the structure of CECs showed vacuolar patchy injury, which became more and more serious from day 1 to day 7, and gradually alleviated from day 7 to day 21, and was similar to that of normal CECs at day 28 (Fig. 5C).

During the whole follow-up period, the immunofluorescence expression of Na⁺/K⁺-ATPase of the corneal endothelium in the MNU + saline group gradually decreased and became negative at day 28, whereas in the MNU + HRS group the expression of Na⁺/K⁺-ATPase decreased significantly from day 1 to day 14, but increased at day 21 and day 28. The difference was statistically significant between the MNU + saline group and the MNU + HRS group ($P < 0.0001$). In every observation window except day 1, the expression of Na⁺/K⁺-ATPase in the MNU + HRS group was higher than that in the MNU + saline group, with statistically significant difference (day 1: $P = 0.3444$; day 3: $P < 0.05$; day 7: $P < 0.05$; day 14: $P < 0.0001$; day 21: $P < 0.0001$; and day 28: $P < 0.0001$; Fig. 6A).

HRS Decreased the Apoptotic CECs Induced by MNU

TUNEL staining showed that a large number of apoptotic cells were found in all layers of cornea in the MNU + saline group at day 21 and day 28 (Fig. 6B). The apoptosis in the MNU + HRS group was significantly slighter than that in
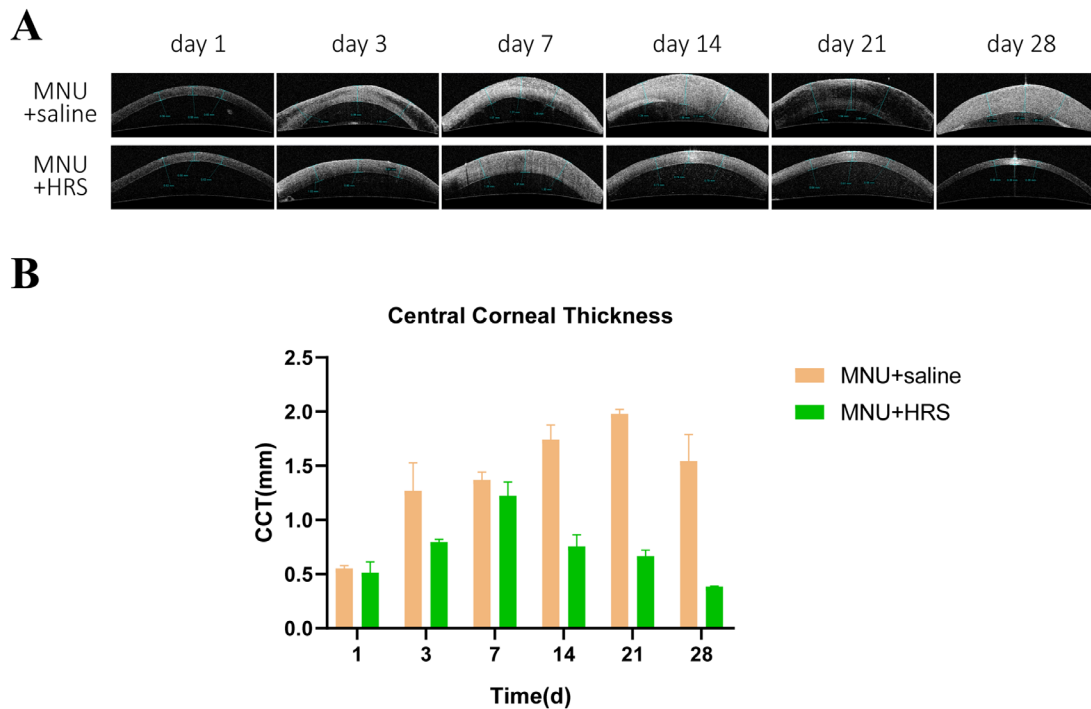
FIGURE 3. AS-OCT examination of rabbit corneas. (**A**) AS-OCT examination showed that the MNU + saline group had more significant corneal edema than the MNU + HRS group. The corneal injury was significantly alleviated in the MNU + HRS group, with smaller CCT compared with the MNU + saline group ($P < 0.0001$, $n = 18$). From day 1 to day 7, CCT increased in both the MNU + saline group and the MNU + HRS group. From day 14, CCT in the MNU + saline group continued to increase, however, corneal edema of rabbits in the MNU + HRS group gradually eased, and finally resembled the normal cornea. (**B**) The mean values of AS-OCT tests were statistically analyzed. There was no statistically significant difference in CCT between the MNU + saline group and the MNU + HRS group at day 1 ($P = 0.5391$) and day 7 ($P = 0.1569$), whereas there were statistically significant differences at day 3 ($P < 0.05$), day 14 ($P < 0.001$), day 21 ($P < 0.0001$), and day 28 ($P < 0.01$).
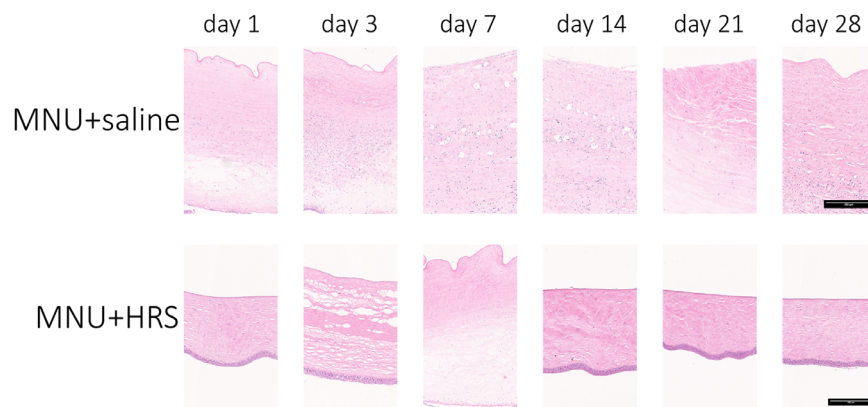

FIGURE 4. H&E staining of rabbit corneas. H&E staining of corneal sections showed that CECs in the MNU + saline group remained absent throughout the observation period, and DM layer detachment was also observed in the MNU + saline group from day 14 after intervention. The CEC damage in the MNU + HRS group was obvious from day 1 to day 7. Evidence of CEC regeneration was observed from day 14. The DM remained unaffected throughout the observation period. Scale bar = 250 µm.

the MNU + saline group, and the difference was statistically significant ($P < 0.0001$, $n = 18$). There were significant differences between the two groups at each time point, suggesting that HRS could significantly reduce MNU-induced CEC apoptosis (day 1: $P < 0.01$; day 3: $P < 0.01$; day 7: $P < 0.0001$; day 14: $P < 0.0001$; day 21: $P < 0.001$; and day 28: $P < 0.0001$).

## HRS Alleviated MNU-Induced Oxidative Stress in Vivo

ROS immunofluorescence staining images showed the expression of ROS in various layers of the cornea, suggesting that the effect of MNU on ROS became stronger and stronger with the passage of time, whereas HRS suspended or even
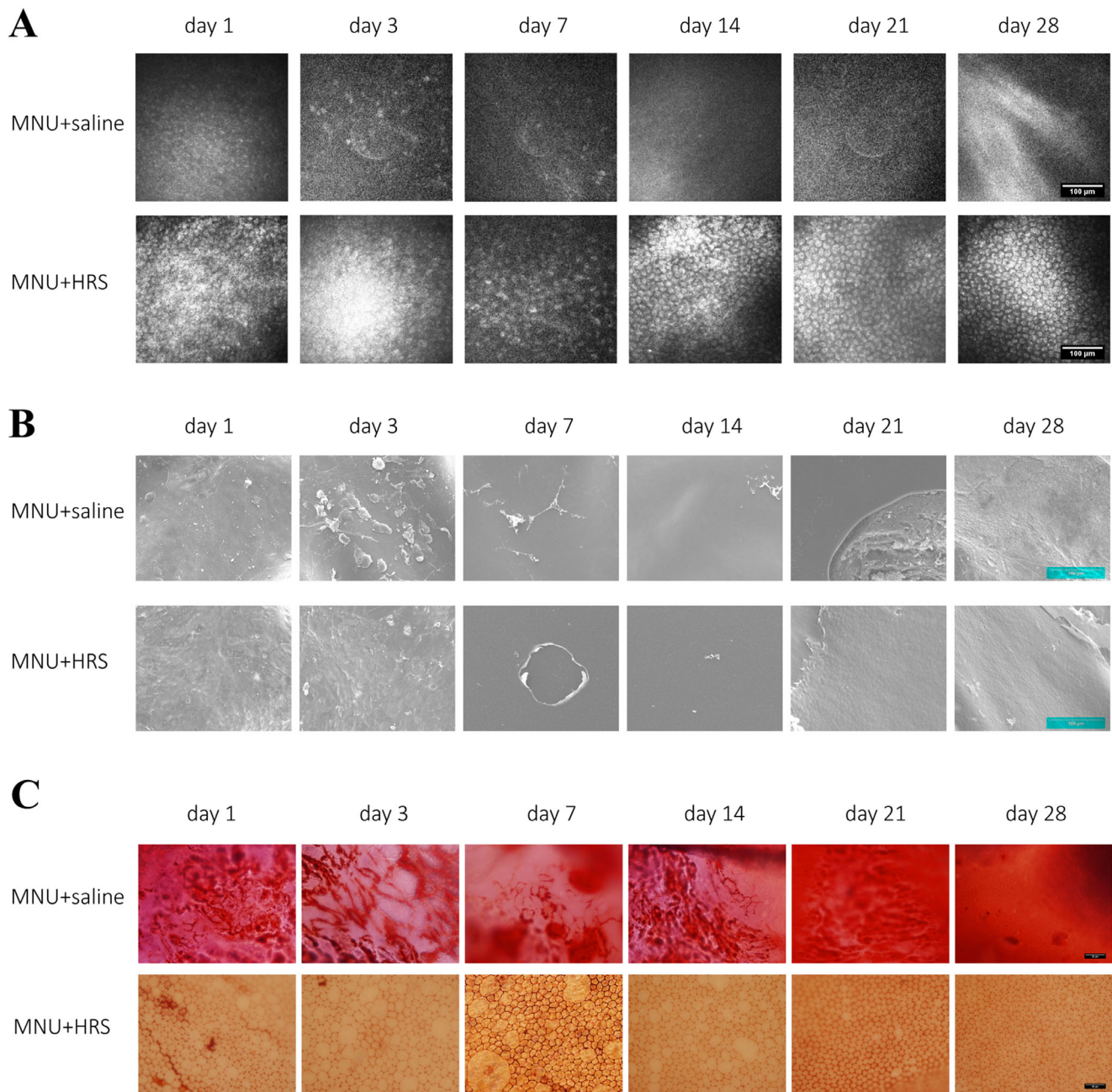
FIGURE 5. **Examinations of corneal endothelium.** (**A**) Representative IVCM images for experimental rabbits. At day 1, sparse and blurred CECs could be seen in the MNU + saline group, and the CECs disappeared from day 3 to day 28. Correspondingly, the CECs in the MNU + HRS group were damaged at a slower speed from day 1 to day 7, showing high reflex, irregular and sparse CECs at day 7. In the MNU + HRS group, CECs regenerated from day 14 after intervention, and images of normal CECs were obtained at day 28, showing uniform hexagonal cells and low reflex on the edge, which meant a return to normal corneal endothelium. Scale bar = 100 μm. (**B**) SEM assay of rabbit corneas. SEM showed that a small number of deformed CECs or cellular residual structures could be seen at day 1 and day 3, no CEC was observed after day 7, and DM injury was observed after day 21 in the MNU + saline group. There were CEC deformation and structural disorder on the inner surface of the cornea in the the MNU + HRS group at day 1 and day 3, and the regeneration of CECs after day 7, but still damage to the DM and CEC layer. Scale bar = 100 μm. (**C**) The corneal specimens were stained with alizarin red S and trypan blue. It was found that CECs were completely ablated, and the cell structure could not be observed in the MNU + saline group during the entire observation period. In the MNU + HRS group, the structure of CECs showed vacuolar patchy injury, which became more and more serious from day 1 to day 7, and gradually alleviated from day 7 to day 21, and was similar to that of normal CECs at day 28. Scale bar = 50 μm.

reversed MNU-induced ROS ($P < 0.0001$, $n = 18$). There were significant differences between the MNU + saline group and the MNU + HRS group at each time point (day 1: $P < 0.01$; day 3: $P < 0.0001$; day 7: $P < 0.001$; day 14: $P < 0.0001$; day 21: $P < 0.0001$; and day 28: $P < 0.0001$; Fig. 6C).
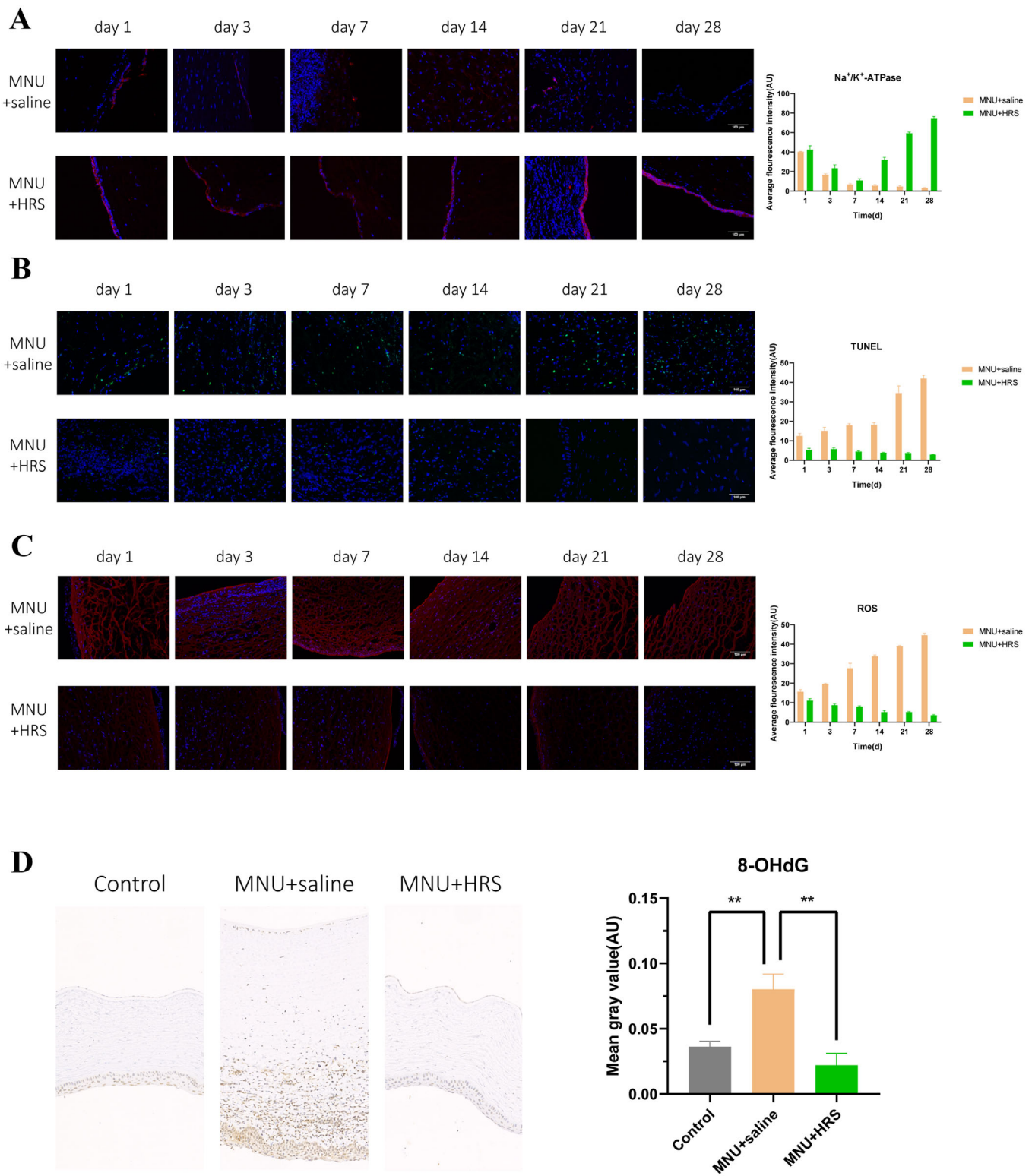
FIGURE 6. Detection of indexes of rabbit corneas. (**A**) The immunofluorescence expression of Na$^+$/K$^+$-ATPase showed a statistically significant difference between the MNU + saline group and the MNU + HRS group. During the whole follow-up period, the immunofluorescence expression of Na$^+$/K$^+$-ATPase of the corneal endothelium in the MNU + saline group gradually decreased and became negative at day 28, whereas the expression in the MNU + HRS group decreased significantly from day 1 to day 14, but increased at day 21 and day 28. The difference was statistically significant between the MNU + saline group and the MNU + HRS group ($P < 0.0001$). In every observation window except day 1, the expression of Na$^+$/K$^+$-ATPase in the MNU + HRS group was higher than that in the MNU + saline group, with a statistically significant difference (day 1: $P = 0.3444$; day 3: $P < 0.05$; day 7: $P < 0.05$; day 14: $P < 0.0001$; day 21: $P < 0.0001$; and day 28: $P < 0.0001$; red: Na$^+$/K$^+$-ATPase; blue: DAPI). Scale bar = 100 μm. (**B**) TUNEL staining of rabbit corneas. TUNEL staining showed that a large number of apoptotic cells were found in all layers of the cornea in the MNU + saline group at day 21 and day 28. The apoptosis

in the MNU + HRS group was significantly slighter than that in the MNU + saline group, and the difference was statistically significant ($P < 0.0001$, $n = 18$). There were significant differences between the two groups at each time point, suggesting that HRS could significantly reduce MNU-induced CEC apoptosis (day 1: $P < 0.01$; day 3: $P < 0.01$; day 7: $P < 0.0001$; day 14: $P < 0.0001$; day 21: $P < 0.001$; and day 28: $P < 0.0001$; *green*: apoptosis; *blue*: DAPI). Scale bar = 100 μm. (**C**) ROS staining of rabbit corneas. ROS immunofluorescence staining images showed the expression of ROS in various layers of the cornea, suggesting that the effect of MNU on ROS became stronger and stronger with the passage of time, whereas HRS suspended or even reversed MNU's induction of ROS ($P < 0.0001$, $n = 18$). There were significant differences between the MNU + saline group and the MNU + HRS group at each time point (day 1: $P < 0.01$; day 3: $P < 0.0001$; day 7: $P < 0.001$; day 14: $P < 0.0001$; day 21: $P < 0.0001$; and day 28: $P < 0.0001$). Scale bar = 100 μm. (**D**) Immunohistochemical assay was used to detect the expression of 8-OHdG in the cornea of New Zealand rabbits at day 28. The expression of 8-OHdG in the MNU + saline group was significantly higher than that in the control group ($P < 0.01$), and the expression of 8-OHdG in the MNU + HRS group was significantly lower than that in the MNU + saline group ($P < 0.01$).
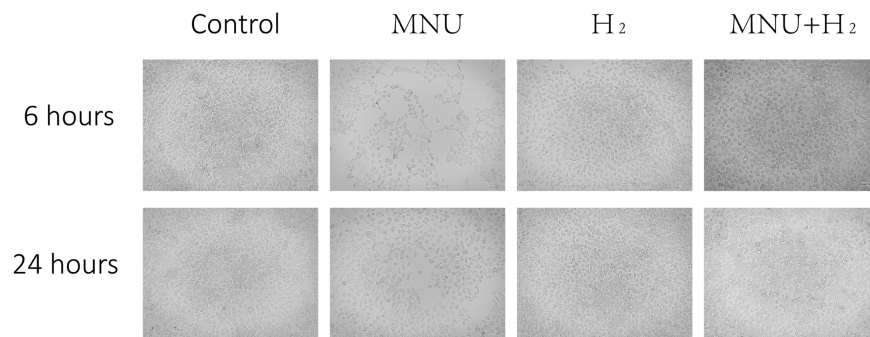
FIGURE 7. **Images of CECs collected at 6 hours and 24 hours.** Cells in the control group adhered to the wall, polygonal, and uniform in size. After co-culture with MNU for 6 hours and 24 hours, the CECs were found significantly sparse than those in the control group. CECs in the MNU group were no longer polygonal in shape. The CECs of the MNU + H$_2$ group were obviously protected by H$_2$ from the killing effect of MNU, although the cell morphology was still very different from that of the control group. Scale bar = 100 μm.

Immunohistochemical assay was used to detect the expression of 8-OHdG in the cornea of New Zealand rabbits at day 28 (Fig. 6D). The expression of 8-OHdG in the MNU + saline group was significantly higher than that in the control group ($P < 0.01$), and the expression of 8-OHdG in the MNU + HRS group was significantly lower than that in the MNU + saline group ($P < 0.01$).

## H$_2$ Reversed the Proliferation Inhibition of MNU on CECs

The B4G12 CEC suspension was put into a 6-well plate and incubated in an incubator. A few hours later, it was observed that the cells adhered to the wall, and were polygonal and uniform in size. After co-culture with MNU for 6 hours and 24 hours, the CECs were found significantly sparse than those in the control group. CECs in the MNU group were no longer polygonal in shape. The CECs of the MNU + H$_2$ group were

obviously protected by H$_2$ from the killing effect of MNU, although the cell morphology was still very different from that of the control group (Fig. 7).

When H$_2$ was pressurized into the medium for 2, 4, 6, 12, 24, 36, and 48 hours, the absorbance of medium containing H$_2$ at 450 nm was higher than that of the control group ($P < 0.0001$, $n = 6$). Considering that the reducibility of H$_2$ significantly changed the results of CCK-8 assay, the culture medium had to change in experimental groups before adding CCK-8 to remove the interference of H$_2$ on the results. The absorbance values of the control group, the MNU group, and the MNU + H$_2$ group were detected. The difference between the control well and the experimental well was divided by the difference between the control well and the blank well to calculate the inhibition rate, indicating that H$_2$ could significantly reduce the cytotoxicity of MNU to cells at 2, 4, 6, 12, and 24 hours after intervention ($P < 0.0001$, $n = 6$; Fig. 8).
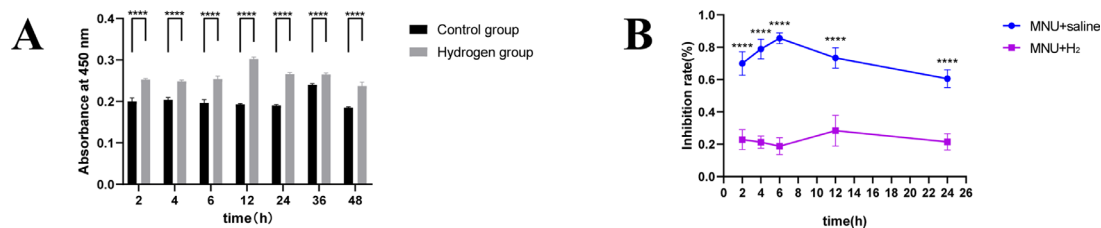
FIGURE 8. **Cell Counting Kit-8 (CCK-8) test.** (**A**) The difference between the control well and the experimental well was divided by the difference between the control well and the blank well to calculate the inhibition rate. When H$_2$ was pressurized into the medium for 2, 4, 6, 12, 24, 36, and 48 hours, the absorbance of medium containing H$_2$ at 450 nm was higher than that of the control group ($P < 0.0001$, $n = 6$). (**B**) The absorbance values of the control group, the MNU group, and the MNU + H$_2$ group were detected. The cytotoxicity inhibition rate was calculated, indicating that H$_2$ could significantly reduce the cytotoxicity of MNU to cells at 2, 4, 6, 12, and 24 hours after intervention ($P < 0.001$).
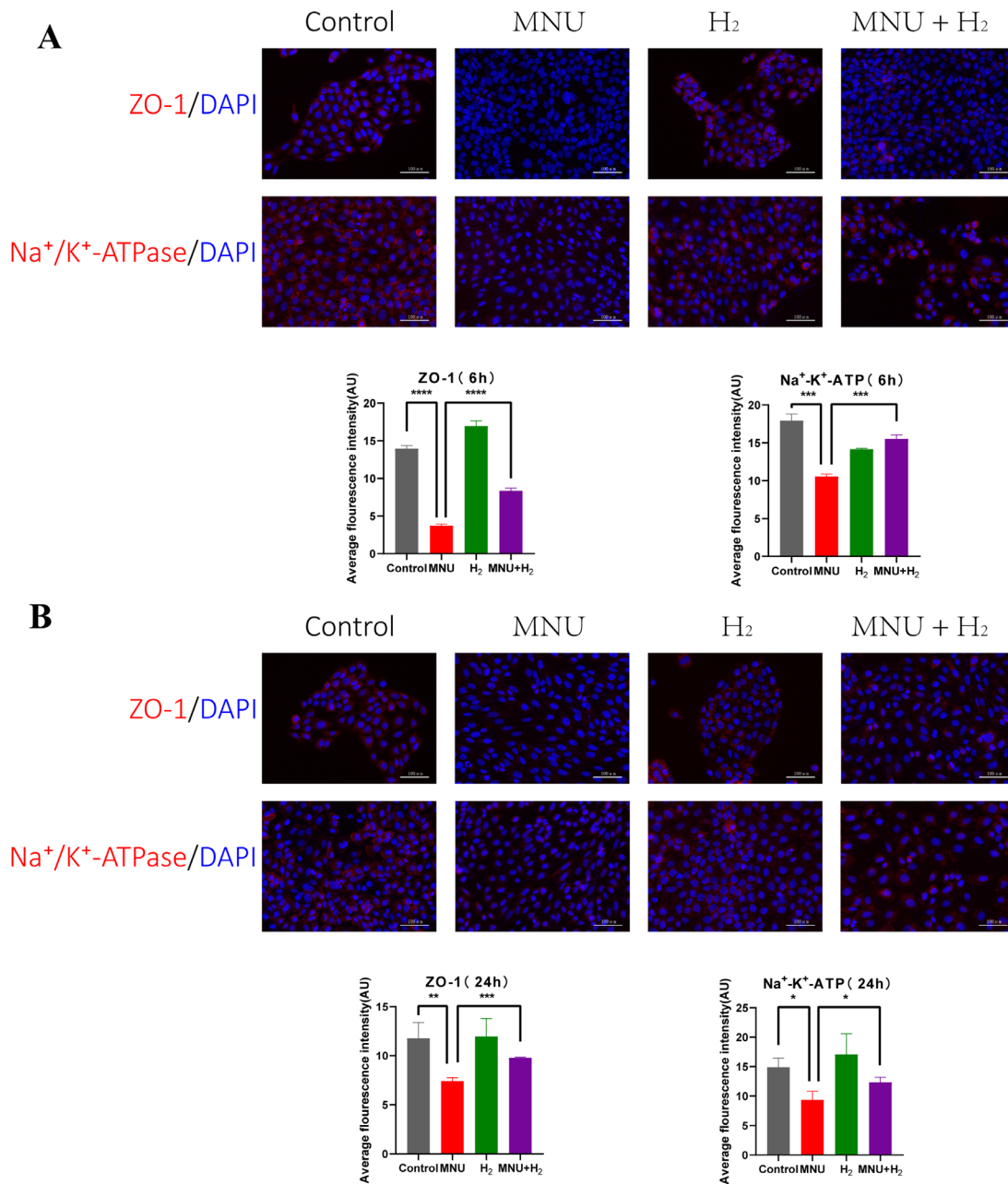
FIGURE 9. Detection of ZO-1 and Na⁺/K⁺-ATPase in CECs. The average fluorescence intensity of immunofluorescence images of CECs was analyzed. (**A**) MNU could reduce the expression of ZO-1 and Na⁺/K⁺-ATPase at 6 hours (ZO-1: $P < 0.0001$, $n = 3$; and Na⁺/K⁺-ATPase: $P < 0.001$, $n = 3$). H₂ could maintain the expression of ZO-1, Na⁺/K⁺-ATPase, and functions of CECs from MNU damage (ZO-1: $P < 0.0001$, $n = 3$; and Na⁺/K⁺-ATPase: $P < 0.001$, $n = 3$). (**B**) MNU could reduce the expression of ZO-1 and Na⁺/K⁺-ATPase at 24 hours (ZO-1: $P < 0.01$, $n = 3$; and Na⁺/K⁺-ATPase: $P < 0.05$, $n = 3$). H₂ could increase the expression of ZO-1 and Na⁺/K⁺-ATPase at 24 hours (ZO-1: $P < 0.001$, $n = 3$; Na⁺/K⁺-ATPase: $P < 0.05$, $n = 3$).

The average fluorescence intensity of immunofluorescence images of CECs was analyzed. As a result, MNU could damage CECs by destroying their physiological functions, which was shown in that MNU could reduce the expression of ZO-1 and Na⁺/K⁺-ATPase (ZO-1 6 hours: $P < 0.0001$; ZO-1 24 hours: $P < 0.01$; Na⁺/K⁺-ATPase 6 hours: $P < 0.001$; and Na⁺/K⁺-ATPase 24 hours: $P < 0.05$; $n = 3$). H₂ could maintain the expression of ZO-1, Na⁺/K⁺-ATPase, and functions of CECs from MNU damage (ZO-1 6 hours: $P < 0.0001$; ZO-1 24 hours: $P < 0.001$; Na⁺/K⁺-ATPase 6 hours: $P < 0.001$; and Na⁺/K⁺-ATPase 24 hours: $P < 0.05$; $n = 3$; Fig. 9).

H₂ Inhibited the Apoptosis Induced by MNU In Vitro

The results of TUNEL assay showed that apoptosis of CECs was accelerated by MNU (TUNEL 6 hours: $P < 0.0001$; and TUNEL 24 hours: $P < 0.0001$; $n = 3$), which was related to the fact that MNU promoted the expression of Bax, caspase-3, and caspase-9, and inhibited the expression of Bcl-2 (Bax 6 hours: $P < 0.0001$; Bax 24 hours: $P < 0.001$; Bcl-2 6 hours: $P = 0.0721$; Bcl-2 24 hours: $P < 0.01$; caspase-3 6 hours: $P < 0.05$; caspase-3 24 hours: $P < 0.001$; caspase-9 6 hours:

$P < 0.01$; and caspase-9 24 hours: $P < 0.05$; $n = 3$). H₂ could reduce apoptosis by inhibiting the expression of Bax, caspase-3, caspase-9, and promoting the expression of Bcl-2 (Bax 6 hours: $P < 0.0001$; Bax 24 hours: $P < 0.05$; Bcl-2 6 hours: $P = 0.4250$; Bcl-2 24 hours: $P < 0.01$; caspase-3 6 hours: $P = 0.0956$; caspase-3 24 hours: $P < 0.001$; caspase-9 6 hours: $P < 0.01$; caspase-9 24 hours: $P < 0.05$; TUNEL 6 hours: $P < 0.0001$; and TUNEL 24 hours: $P < 0.01$; $n = 3$; Figs. 10A, 10B).

Western blot (WB) was conducted on the related indicators of apoptosis of CECs. It was suggested that MNU could significantly increase Bax and decrease Bcl-2, with statistical significance (Bax: $P < 0.001$; Bcl-2: $P < 0.01$; $n = 3$). Apoptotic markers were detected and both caspase-3 and caspase-9 were activated by MNU (caspase-3: $P < 0.001$; and caspase-9: $P < 0.01$; $n = 3$). H₂ could antagonize the pro-apoptotic effect of MNU by reducing Bax and increasing Bcl-2 (Bax: $P < 0.01$; and Bcl-2: $P < 0.01$; $n = 3$), and changes of caspase-3 and caspase-9 also suggested the inhibitory effect of H₂ on the pro-apoptotic properties of MNU (caspase-3: $P < 0.01$; and caspase-9: $P < 0.01$; $n = 3$; Fig. 10C).

H₂ can Inhibit the Oxidative Stress Induced by MNU in CECs

The absorbance of MDA, catalase, and GSH in all groups was measured by spectrophotometer at 6 hours and 24 hours, and the MDA content, catalase activity, and GSH activity were calculated according to the instructions of the kits (Fig. 11). There were statistically significant differences in the three indexes between the MNU group and the control group (MDA 6 hours: $P < 0.0001$; MDA 24 hours: $P < 0.0001$; catalase 6 hours: $P < 0.0001$; catalase 24 hours: $P < 0.0001$; GSH 6 hours: $P < 0.05$; and GSH 24 hours: $P < 0.001$; $n = 3$). Compared with the MNU group, H₂ decreased MDA content, increased catalase activity, and GSH activity, with statistical significance (MDA 6 hours: $P < 0.05$; MDA 24 hours: $P < 0.0001$; catalase 6 hours: $P < 0.0001$; catalase 24 hours: $P < 0.001$; GSH 6 hours: $P < 0.05$; and GSH 24 hours: $P < 0.01$; $n = 3$).

H₂ Inhibited the Activation of NF*κ*B/NLRP3 Pathway Induced by MNU in CECs

It is generally believed that activation of the NF*κ*B/NLRP3 pathway is associated with cellular inflammatory response. Immunofluorescence staining was used to study the effect of MNU on NF*κ*B/NLRP3 pathway of CECs. Nuclear translocation of NF*κ*B p65 was observed in the MNU group. MNU enhanced the fluorescence of NF*κ*B p65, nucleotide binding, and oligomerization domain-like receptor family pyrin domain-containing 3 (NLRP3), ASC, caspase-1, and IL-1*β* with statistical significance (NF*κ*B p65 6 hours: $P < 0.01$; NF*κ*B p65 24 hours: $P < 0.001$; NLRP3 6 hours: $P < 0.05$; NLRP3 24 hours: $P = 0.1477$; ASC 6 hours: $P < 0.001$; ASC 24 hours: $P < 0.001$; caspase-1 6 hours: $P < 0.001$; caspase-1 24 hours: $P < 0.001$; IL-1*β* 6 hours: $P < 0.05$; and IL-1*β* 24 hours: $P < 0.05$; $n = 3$). However, H₂ suppressed the nuclear translocation of NF*κ*B p65 induced by MNU, and inhibited the expression of NF*κ*B/NLRP3 pathway (NF*κ*B p65 6 hours: $P < 0.001$; NF*κ*B p65 24 hours: $P < 0.0001$; NLRP3 6 hours: $P < 0.01$; NLRP3 24 hours: $P = 0.3106$; ASC 6 hours: $P < 0.001$; ASC 24 hours: $P < 0.01$; caspase-1 6 hours: $P = 0.1961$; caspase-1 24 hours: $P < 0.01$; IL-1*β* 6 hours: $P = 0.5910$; and IL-1*β* 24 hours: $P < 0.05$; $n = 3$; Figs. 12A, 12B).

NF*κ*B p65 was analyzed by quantitative PCR. It was found that the expression of NF*κ*B p65 of CECs in the MNU group was increased compared with the control group, and the difference was statistically significant (6 hours: $P < 0.001$; and 24 hours: $P < 0.0001$; $n = 3$; Fig. 12C). WB showed that the content of NF*κ*B p65 shared by cytoplasm and nucleus of CECs in the MNU group was significantly higher than that in the control group ($P < 0.05$, $n = 3$; Fig. 12D). Both PCR and WB results showed that H₂ did not significantly reduce the expression of NF*κ*B p65 (PCR 6 hours: $P = 0.2008$; PCR 24 hours: $P = 0.2685$; and WB: $P = 0.0526$; $n = 3$; see Figs. 12C, 12D).

## H₂ Inhibited the Activation of FOXO3a/p53/p21 Pathway of MNU in CECs

The immunofluorescence images of CECs showed that MNU activated FOXO3a/p53/p21 pathway represented by promoting FOXO3a nuclear translocation and expression of FOXO3a, p53, and p21 (FOXO3a 6 hours: $P < 0.0001$; FOXO3a 24 hours: $P < 0.0001$; p53 6 hours: $P < 0.01$; p53 24 hours: $P < 0.0001$; p21 6 hours: $P < 0.0001$; and p21 24 hours: $P < 0.0001$; $n = 3$), whereas H₂ had an inhibitory effect on this pathway (FOXO3a 6 hours: $P < 0.001$; FOXO3a 24 hours: $P < 0.001$; p53 6 hours: $P < 0.05$; p53 24 hours: $P < 0.001$; p21 6 hours: $P < 0.001$; and p21 24 hours: $P < 0.01$; $n = 3$; Figs. 13A, 13B).

Quantitative PCR analysis of FOXO3a was performed. It was found that the expression of FOXO3a of CECs in MNU group was higher than that of the control group, and the difference was statistically significant (6 hours: $P<0.0001$; and 24 hours: $P<0.01$; $n = 3$). H₂ reduced the activation effect of MNU, but the difference was not statistically significant (6 hours: $P = 0.2390$; and 24 hours: $P = 0.6756$; $n = 3$; Fig. 13C). WB demonstrated that MNU could significantly induce the expression of FOXO3a ($P < 0.0001$, $n = 3$), but this pathological process was inhibited by H₂ ($P<0.0001$, $n = 3$; Fig. 13D).

DISCUSSION

Corneal endothelial decompensation leads to severe visual impairment, which brings many difficulties in treatment. Currently, the only treatment for corneal endothelial decompensation is corneal transplantation using a donor cornea.[8] Over the past decade, Descemet's stripping automated endothelial keratoplasty (DSAEK) and Descemet's membrane endothelial keratoplasty (DMEK) are safer and more effective compared with traditional penetrating keratoplasty (PK). However, disadvantages of these endothelial keratoplasty techniques, such as difficulty of the actual surgical techniques, acute and chronic cell loss, and a shortage of donor corneas, make it very valuable to find new treatment methods.[29,30]

H₂, as a safe and effective medical gas with little side effects, could be used for the treatment of many diseases. H₂ could regulate signal transduction through a variety of pathways. However, its main molecular targets have not been identified. In addition to selective antioxidant and anti-inflammatory effects, H₂ could exert anti-apoptotic effects by up- or downregulating apoptosis-related factors, such as caspase-3, Bcl-2, and Bax.[18] As far as we know, this is the first
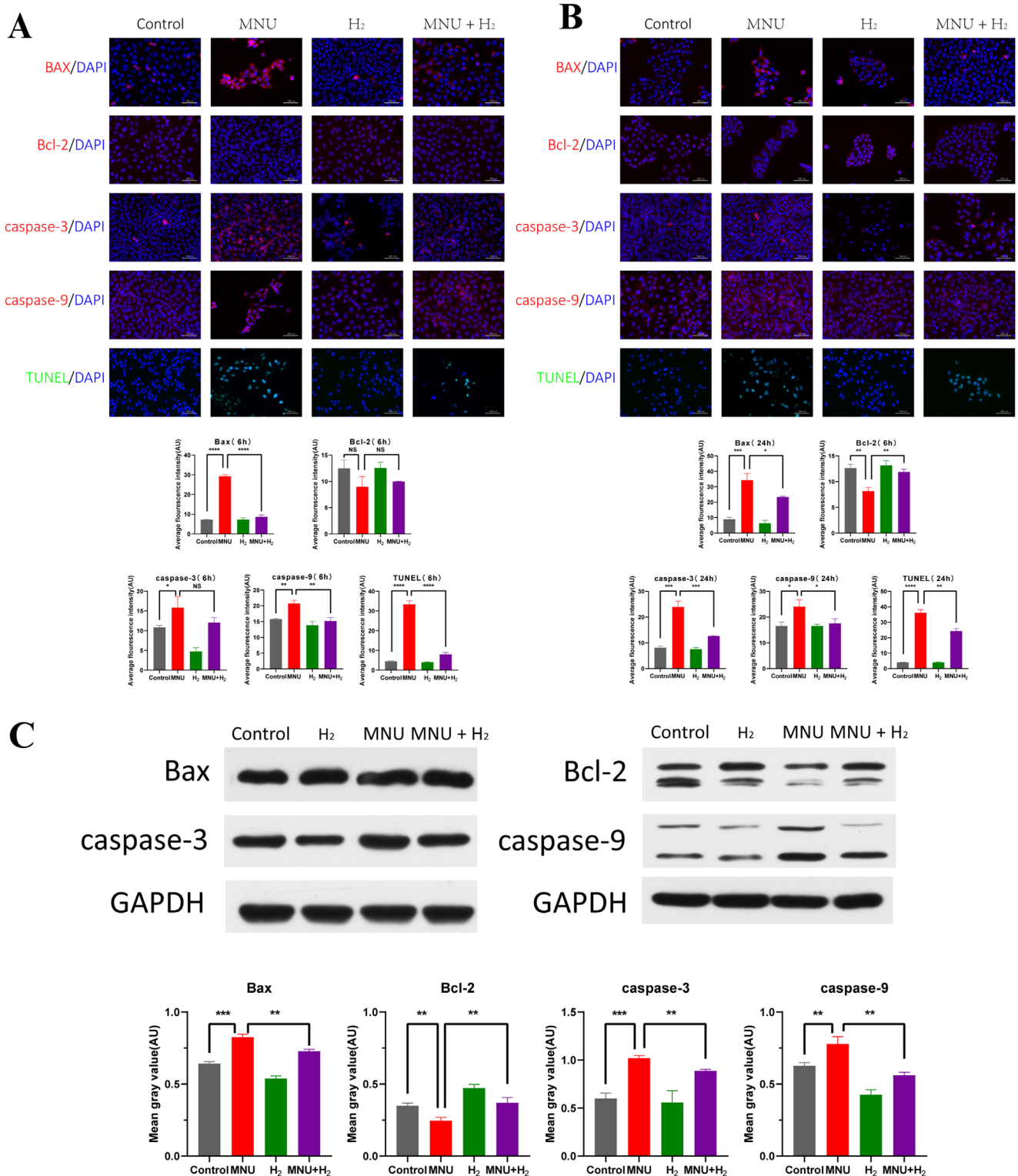
FIGURE 10. **Detection of apoptosis in CECs.** (**A**) The results of TUNEL assay showed that apoptosis of CECs was accelerated by MNU at 6 hours ($P < 0.0001$, $n = 3$), which was related to the fact that MNU promoted the expression of Bax, caspase-3, and caspase-9 and inhibited the expression of Bcl-2 (Bax: $P < 0.0001$, $n = 3$; Bcl-2: $P = 0.0721$, $n = 3$; caspase-3: $P < 0.05$, $n = 3$; and caspase-9: $P < 0.01$, $n = 3$). H₂ could reduce apoptosis by inhibiting the expression of Bax, caspase-3, and caspase-9, and promoting the expression of Bcl-2 at 6 hours (Bax: $P < 0.0001$, $n = 3$; Bcl-2: $P = 0.4250$, $n = 3$; caspase-3: $P = 0.0956$, $n = 3$; caspase-9: $P < 0.01$, $n = 3$; and TUNEL: $P < 0.0001$, $n = 3$). (**B**) The results of TUNEL assay showed that apoptosis of CECs was accelerated by MNU at 24 hours ($P < 0.0001$, $n = 3$), which was related to the fact that MNU promoted the expression of Bax, caspase-3, and caspase-9 and inhibited the expression of Bcl-2 (Bax: $P < 0.001$, $n = 3$; Bcl-2: $P < 0.01$, $n = 3$; caspase-3: $P < 0.001$, $n = 3$; and caspase-9: $P < 0.05$, $n = 3$). H₂ could reduce apoptosis by inhibiting the expression of Bax, caspase-3, and caspase-9 and promoting the expression of Bcl-2 at 24 hours (Bax: $P < 0.05$, $n = 3$; Bcl-2: $P < 0.01$, $n = 3$; caspase-3:

P < 0.001, *n* = 3; caspase-9: *P* < 0.05, *n* = 3; and TUNEL: *P* < 0.01, *n* = 3). (**C**) WB was conducted on the related indicators of apoptosis of CECs. It was suggested that MNU could significantly increase Bax and decrease Bcl-2, with statistical significance (Bax: *P* < 0.001, *n* = 3; and Bcl-2: *P* < 0.01, *n* = 3). Apoptotic markers were detected and both caspase-3 and caspase-9 were activated by MNU (caspase-3: *P* < 0.001, *n* = 3; and caspase-9: *P* < 0.01, *n* = 3). H$_2$ could antagonize the pro-apoptotic effect of MNU by reducing Bax and increasing Bcl-2 (Bax: *P* < 0.01, *n* = 3; and Bcl-2: *P* < 0.01, *n* = 3), and changes of caspase-3 and caspase-9 also suggested the inhibitory effect of H$_2$ on the pro-apoptotic properties of MNU (caspase-3: *P* < 0.01, *n* = 3; and caspase-9: *P* < 0.01, *n* = 3).
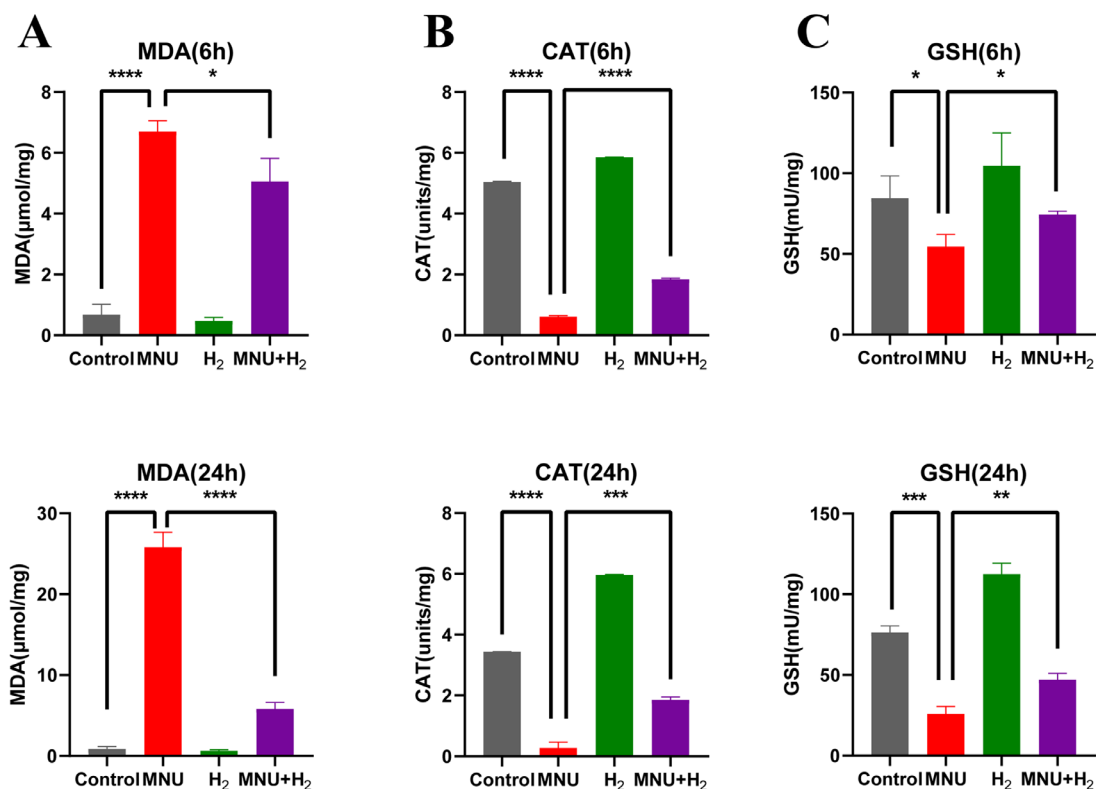

FIGURE 11. Detection of the absorbance of MDA, catalase, and GSH in CECs at 6 hours and 24 hours. The MDA content, catalase activity, and GSH activity were calculated according to the instructions of the kits. There were statistically significant differences in three indexes between the MNU group and the control group (MDA 6 hours: *P* < 0.0001; MDA 24 hours: *P* < 0.0001; catalase 6 hours: *P* < 0.0001; catalase 24 hours: *P* < 0.0001; GSH 6 hours: *P* < 0.05; and GSH 24 hours: *P* < 0.001). Compared with the MNU group, HRS decreased the MDA content, and increased the catalase activity and GSH activity, with statistical significance (MDA 6 hours: *P* < 0.05; MDA 24 hours: *P* < 0.0001; catalase 6 hours: *P* < 0.0001; catalase 24 hours: *P* < 0.001; GSH 6 hours: *P* < 0.05; and GSH 24 hours: *P* < 0.01; *n* = 3).

time that the therapeutic effects of H$_2$ on the animal model and cell model of MNU-induced CEC injury were investigated.

Our team established a mammalian corneal endothelial decompensation model induced by anterior chamber injection of MNU for the first time to simulate the damage of CECs induced by phacoemulsification or TASS, and confirmed its effectiveness and safety.[11] For economic and ethical reasons, New Zealand rabbits were still used as experimental animals for treating MNU-induced corneal endothelial injury with H$_2$. The dosage of MNU was 3.0 mg/kg, which could cause corneal endothelial decompensation, DM injury, and severe corneal edema. The characteristics of large eyeballs and easy feeding of rabbits are very helpful to our experiment. The high concentration of MNU we selected reduced the interference brought by the powerful regeneration ability of rabbit CECs to the experimental results.[11,31] Using IVCM, SEM, and section staining, the corneal endothelium was damaged on the first day after MNU injection into the rabbit's anterior

chamber and irreparably worsened over the following 28 days. The use of HRS allowed CECs to regenerate around the 14th day after the intervention, and basically returned to normal at day 28, and protected the DM throughout the observation. Both slit lamp microscopy and AS-OCT showed that HRS gave animal models the opportunity to reduce or reverse MNU-induced corneal edema.

The current markers used for preclinical identification of healthy CECs were not unique to these cells or their lineages.[32,33] The unique functions of CECs include monolayer tight junction and humoral barrier, which are vulnerable to disruption by corneal endothelial diseases, such as FECD, as indicated by the expression of Na$^+$/K$^+$-ATPase and Zonula occuludens-1 (ZO-1), respectively. In CECs, Na$^+$/K$^+$-ATPase, together with all other ion channels, established a membrane potential of approximately 30 mV and participated in the formation of a local hypertonic gradient.[32,33] The mechanism has not yet been elucidated. The ZO-1 protein, also known as an atresia, is usually abundant in the
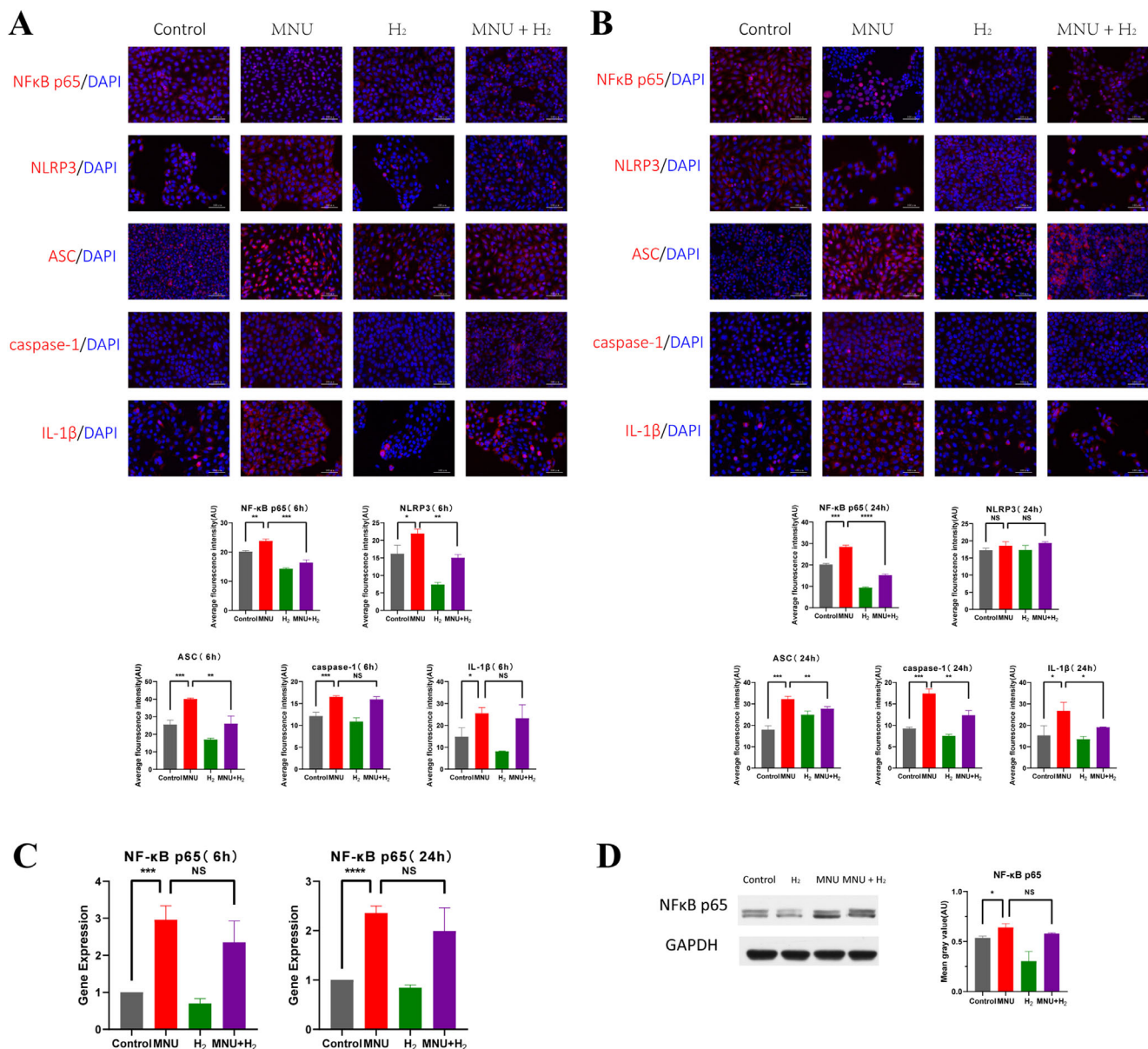
FIGURE 12. Detection of the NFκB/NLRP3 pathway in CECs. (A) Immunofluorescence staining was used to study the effect of MNU on the NFκB/NLRP3 pathway of CECs at 6 hours. Nuclear translocation of NFκB p65 was observed in the MNU group. MNU enhanced the fluorescence of NFκB p65, NLRP3, ASC, caspase-1, and IL-1β with statistical significance (NFκB p65: $P<0.01$, $n = 3$; NLRP3: $P<0.05$, $n = 3$; ASC: $P<0.001$, $n = 3$; caspase-1: $P<0.001$, $n = 3$; and IL-1β: $P<0.05$, $n = 3$). However, H₂ suppressed the nuclear translocation of NFκB p65 induced by MNU, and inhibited the expression of the NFκB/NLRP3 pathway (NFκB p65: $P<0.001$, $n = 3$; NLRP3: $P<0.01$, $n = 3$; ASC: $P<0.01$, $n = 3$; caspase-1: $P = 0.1961$, $n = 3$; and IL-1β: $P = 0.5910$, $n = 3$). **(B)** Immunofluorescence staining was used to study the effect of MNU on the NFκB/NLRP3 pathway of CECs at 24 hours. Nuclear translocation of NFκB p65 was observed in the MNU group. MNU enhanced the fluorescence of NFκB p65, NLRP3, ASC, caspase-1, and IL-1β with statistical significance (NFκB p65: $P<0.001$, $n = 3$; NLRP3: $P = 0.1477$, $n = 3$; ASC: $P<0.001$, $n = 3$; caspase-1: $P<0.001$, $n = 3$; and IL-1β: $P<0.05$, $n = 3$). However, H₂ suppressed the nuclear translocation of NFκB p65 induced by MNU, and inhibited the expression of the NFκB/NLRP3 pathway (NFκB p65: $P<0.0001$, $n = 3$; NLRP3: $P = 0.3106$, $n = 3$; ASC: $P<0.01$, $n = 3$; caspase-1: $P<0.01$, $n = 3$; and IL-1β: $P<0.05$, $n = 3$). **(C)** NFκB p65 was analyzed by quantitative PCR. It was found that the expression of NFκB p65 of CECs in the MNU group was increased compared with the control group, and the difference was statistically significant (6 hours: $P<0.001$, $n = 3$; and 24 hours: $P<0.0001$, $n = 3$). H₂ did not significantly reduce the expression of NFκB p65 (6 hours: $P = 0.2008$, $n = 3$; and 24 hours: $P = 0.2685$, $n = 3$). **(D)** WB showed that the content of NFκB p65 shared by cytoplasm and nucleus of CECs in the MNU group was significantly higher than that in the control group ($P<0.05$, $n = 3$). H₂ did not significantly reduce the expression of NFκB p65 ($P = 0.0526$, $n = 3$).

epithelium and endothelium. The main role of tight junctions is to prevent the mixing of basolateral molecules and apical molecules, thus maintaining the polarity of the cell. The ZO-1 was expressed and responsible for passive diffusion of nutrients from the anterior chamber to the cornea.[32]

In this experiment, it could be seen by cell images that the cell connections in the MNU group were extensively destroyed, the degree of cell population dispersion was increased, and the polygon morphology of normal CECs was lost. The physiological functions of CECs were restored to
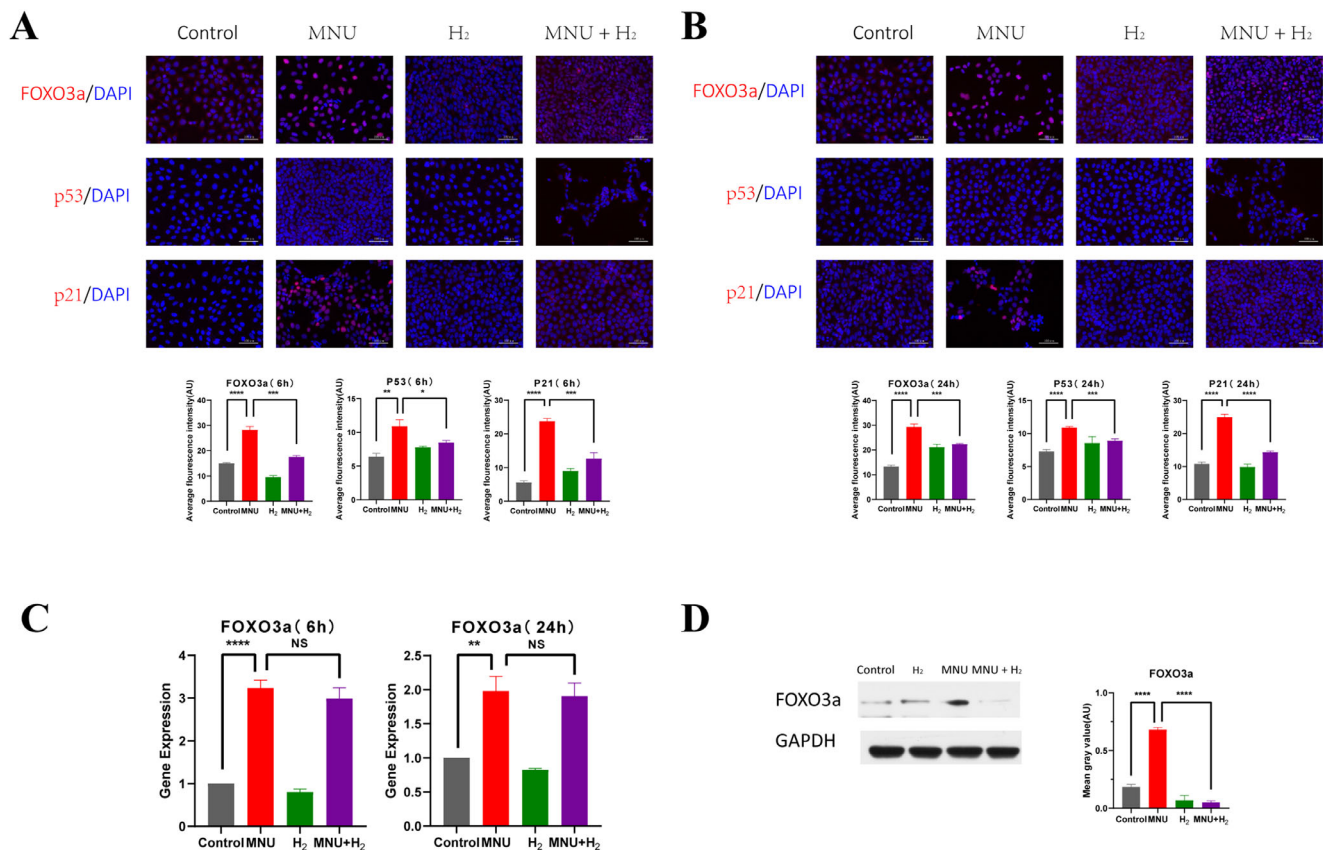
FIGURE 13. Detection of the FOXO3a/p53/p21 pathway in CECs. (**A**) The immunofluorescence images of CECs showed that MNU activated the FOXO3a/p53/p21 pathway represented by promoting FOXO3a nuclear translocation and expression of FOXO3a, p53, and p21 at 6 hours (FOXO3a: $P<0.0001$, $n = 3$; p53: $P < 0.01$, $n = 3$; and p21: $P < 0.0001$, $n = 3$), whereas H$_2$ had an inhibitory effect on this pathway (FOXO3a: $P < 0.001$, $n = 3$; p53: $P < 0.05$, $n = 3$; and p21: $P < 0.001$, $n = 3$). (**B**) The immunofluorescence images of CECs showed that MNU activated the FOXO3a/p53/p21 pathway represented by promoting FOXO3a nuclear translocation and expression of FOXO3a, p53, and p21 at 24 hours (FOXO3a: $P < 0.0001$, $n = 3$; p53: $P<0.0001$, $n = 3$; and p21: $P < 0.0001$, $n = 3$), whereas H$_2$ had an inhibitory effect on this pathway (FOXO3a: $P < 0.001$, $n = 3$; p53: $P < 0.001$, $n = 3$; and p21: $P < 0.01$, $n = 3$). (**C**) Quantitative PCR analysis of FOXO3a was performed. It was found that the expression of FOXO3a of CECs in MNU group was higher than that of the control group, and the difference was statistically significant (6 hours: $P < 0.0001$, $n = 3$; and 24 hours: $P < 0.01$, $n = 3$). H$_2$ reduced the activation effect of MNU, but the difference was not statistically significant (6 hours: $P = 0.2390$, $n = 3$; and 24 hours: $P = 0.6756$, $n = 3$). (**D**) WB demonstrated that MNU could significantly induce the expression of FOXO3a ($P < 0.0001$, $n = 3$), but this pathological process was inhibited by H$_2$ ($P < 0.0001$, $n = 3$).

some extent in the MNU + H$_2$ group. It is consistent with changes of Na$^+$/K$^+$-ATPase and ZO-1 in the cell model. MNU also reduced the expression of Na$^+$/K$^+$-ATPase of CECs in animals.

Apoptosis is a highly conserved process of cell death that is tightly regulated to eliminate unwanted cells and potentially harmful cells with DNA damage. Physiologically, apoptosis can maintain cell homeostasis. However, excessive apoptosis is associated with many pathologies, such as chronic inflammation, cancer, and degenerative diseases of various organs.[34] The inducers of apoptosis come from internal signals or environmental changes, including ROS, heat shock, viral infection, hypoxia, environmental pollutants, and chemotherapy drugs, etc.[35] TUNEL assay was performed in animal and cell models. It was observed that H$_2$ significantly reduced the apoptotic level of CECs exposed to MNU both in vivo and in vitro, strongly suggesting the anti-apoptotic effect of H$_2$ (Fig. 14).

Cell lines were used to verify changes in apoptosis-related factors in CECs in the presence of MNU or H$_2$. The Bax/Bcl-2 pathway can regulate the process of cell apoptosis.[36] The release of mitochondrial cytochrome C is inhibited by the anti-apoptotic protein Bcl-2 and promoted by the pro-apoptotic protein Bax, because the former inhibits oxygen free radical-mediated membrane damage, whereas the latter changes the permeability of the mitochondrial membrane.[37] The increase of apoptosis can be inferred by the increase of Bax expression and the decrease of Bcl-2 expression.[38] Apoptosis is closely related to the activation of caspases, of which caspase-9 is the initiator and caspase-3 is the executor. They work together to participate in a series of cellular events that lead to DNA breakage. Excessive ROS activates caspase-9, leads to the initiation of caspase-3-mediated cascade reaction, and finally leads to apoptosis.[39] H$_2$ played an anti-apoptotic role by upregulating Bcl-2 or downregulating Bax, and inhibited cell apoptosis by regulating signal transduction within and between specific pathways.[18] When CECs were co-cultured with MNU, the increased expression of Bax and the decreased expression of Bcl-2 proved that the apoptosis pathway of CECs was activated. The increased expression of caspase-9 and caspase-3 indicated that the process of apoptosis was accelerated. However, H$_2$ played the opposite role.
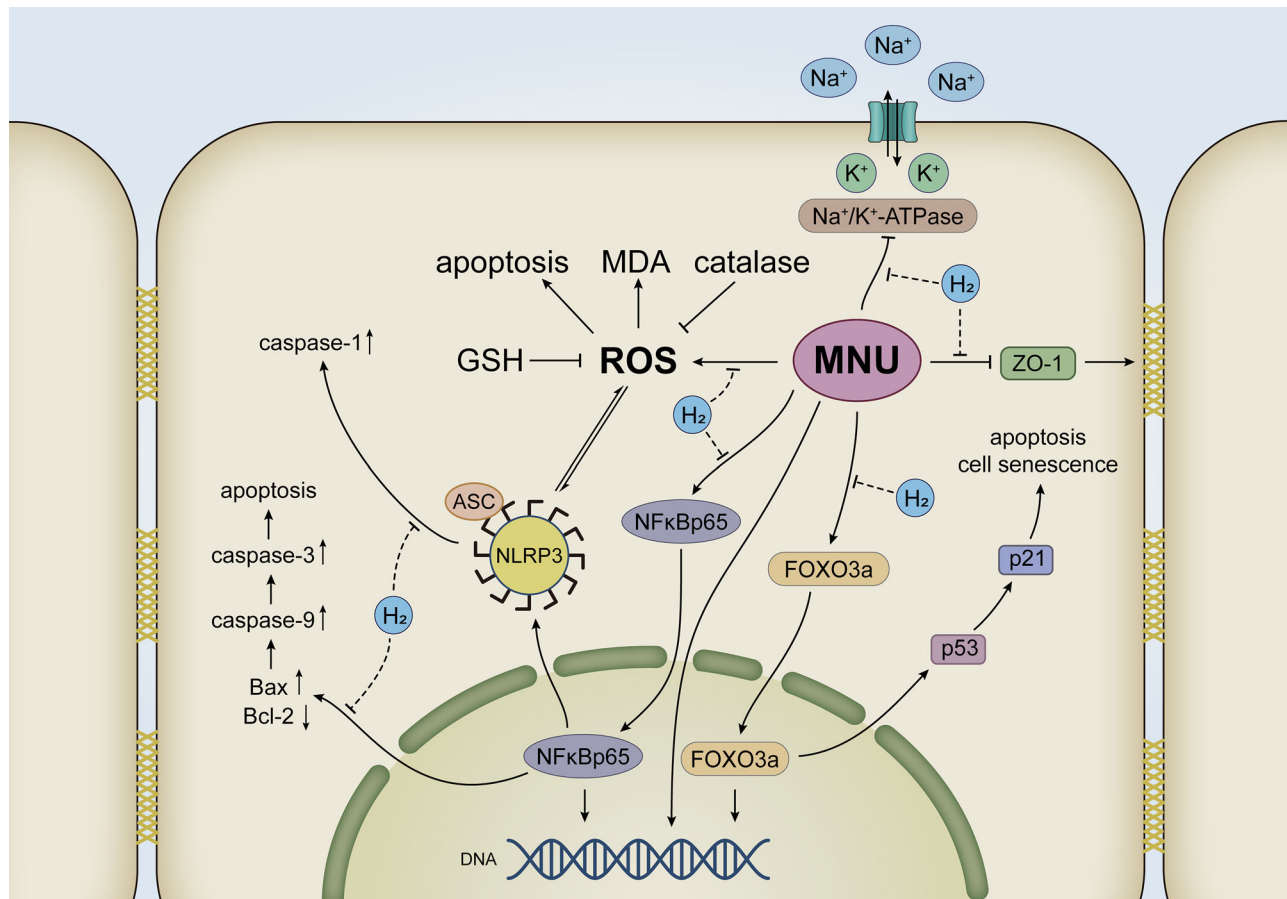
FIGURE 14. **The antiapoptotic effect of H$_2$ in attenuating MNU induced corneal endothelial injury.** The adverse effects of MNU on the physiological functions of CECs were alleviated by H$_2$ increasing Na$^+$/K$^+$-ATPase and ZO-1. H$_2$ decreased the MDA content and increased catalase activity and GSH activity to alleviate oxidative stress injury caused by MNU. H$_2$ was associated with the inhibition of the NF-κB/NLRP3 pathway and the FoxO3a/p53/p21 pathway. As a result, H$_2$ reduced the apoptosis of CECs induced by MNU.

Apoptosis is usually mediated by ROS, which plays a central role in cell signal transduction and the major pathways of apoptosis mediated by mitochondria, death receptors, and endoplasmic reticulum (ER).[34] Under physiological conditions, ROS acts as signaling molecules to regulate cell growth, cell adhesion to other cells, differentiation, senescence, and apoptosis.[40] Oxidative stress can be characterized by excessive ROS, which is a disaster for normal cells, but fortunately eyes have a variety of antioxidant defense systems.[41,42] The antioxidant function of H$_2$ can also play a role in corneal cells, mainly because H$_2$, as an antioxidant, can resist or reverse the pathological development caused by oxidative stress, showing the anti-apoptotic effect.[18,43]

In vivo, H$_2$ selectively neutralized the most reactive ROS, hydroxyl radical ($\cdot$OH) and peroxynitrite (ONOO$^-$), without affecting other functional ROS, such as superoxide (O^{2-}) and hydrogen peroxide (H$_2$O$_2$), which not only reduced adverse reactions, but also improved efficiency of antioxidation.[6,18,19,23,27,44] So far, researches reporting that the incidence of ROS-related diseases decrease with the use of HRS have involved both in vitro and in vivo studies.[6,20,43,45,46] In human diseases and rodent models, H$_2$ reduced the expression of various oxidative stress markers, such as myeloperoxidase, MDA, 8-OHdG, etc.[18] MDA content, GSH activity, and catalase activity can reflect the level of oxidative stress and evaluate the effect of drugs on oxidative stress. MDA

is one of the peroxides that indirectly reflect the generation of free radicals. The increasing effect of MNU on it and the decreasing effect of H$_2$ on it can reflect the direction of their intervention on oxidative stress of CECs.[47] Catalase and GSH can effectively scavenge free radicals, and play an important role in maintaining the redox status of normal cells, and MNU can reduce antioxidant enzymes, such as reduced glutathione and weaken the antioxidant defense system.[36,42,48] However, H$_2$ reduces oxidative stress by repressing the production of ROS and increasing the activity of glutathione peroxidase (GSH-Px), thus decreasing the content of MDA. The detection of these three indicators in the CEC model is the verification of MNU triggering oxidative stress damage and H$_2$-reducing oxidative stress damage. The 8-OHdG is another marker of oxidative stress.[6] In this experiment, immunohistochemical staining of 8-OHdG was performed on rabbit corneas, showing pro-oxidation effect of MNU and antioxidant status of HRS. DHE could freely enter living cells, oxidized by intracellular ROS, affecting DNA, and producing red fluorescence.[49] We examined the rabbit corneas, and ROS levels were intuitively reflected. It showed that MNU induced ROS in a time-dependent manner, and HRS suspended or even reversed ROS. It suggested that H$_2$ had the potential as a preventive and therapeutic antioxidant, exerting the anti-apoptotic effect in vivo.

As an upstream pathway of the Bax/Bcl-2 pathway, the NF-κB pathway can affect cell apoptosis.[34] Excessive oxidative stress is associated with the NF-κB pathway, the NLRP3 pathway, and the caspase signaling pathway, through which apoptosis are induced.[37] By binding to them, inhibitors of NF-κB (IκB) force the NF-κB transcription factor family to remain in the cytoplasm in an inactive form. When the NF-κB pathway is activated, IκBα is phosphorylated, ubiquitinated, and degraded by proteasome, which releases NF-κB dimer into the nucleus, initiates transcription, and expresses inflammatory mediators (such as IL-1, IL-6, TNF, and IL-23) and related proteins that are involved in immune response, inflammatory response, and tumor growth.[36,50–54] P65 is a member of the NF-κB family and is inactive in unstimulated cells. The binding of heterodimer containing p65 to DNA after cellular stimulation may result in increased gene expression.[55] The results of WB and PCR confirmed the upregulation of NF-κB p65 in CECs exposed to MNU. Immunofluorescence data further confirmed the transfer of NF-κB p65 from the cytoplasm to the nucleus, suggesting that MNU disturbance in CECs is related to the activation of the NF-κB signaling pathway.

Recently, it has been reported that the NF-κB pathway was involved in the initiation of NLRP3 inflammasome.[51,56,57] NLRP3 inflammasome, as an important component of the innate immune system, is the most thoroughly studied inflammasome. In combination with the aptamer apoptosis-associated speck-like protein containing CARD (ASC), it mediates the activation of cysteine aspartate proteinase-1 (caspase-1) and the secretion of proinflammatory cytokines including IL-1β and IL-18.[21,51,58–64] Activation signals can be provided by a variety of extracellular stimuli or molecules, including microbial toxins, as well as cellular damage events, such as mitochondrial dysfunction and ROS production. Among them, intracellular ROS and NLRP3 inflammasomes are mutually promoted.[51,58,65] Studies have shown that both corneal and conjunctival epithelial cells harbor functional NLRP3 inflammasomes.[60,66] Due to the difference between infectious and noninfectious lesions, different corneal diseases may be associated with variation in expression of nucleotide binding and oligomerization domain-like receptor (NLR).[67] In our study, the immunofluorescence staining of ASC, caspase-1, and IL-1β of CECs were all enhanced under MNU, whereas they were weakened under H₂, indicating that the function of NLRP3 inflammasomes could be activated by MNU and inhibited by H₂.

Therefore, H₂ may belong to those compounds that inhibit NLRP3 inflammasomes, reduce the release of cytokines, alleviate mitochondrial dysfunction and abnormal inflammatory response, and treat organ damage by regulating cellular redox state and NF-κB pathway.[18,21,41,56,59,68,69] H₂ plays a role by regulating the expression of various genes, including NF-κB and signal transduction within and between specific pathways.[18] Wu et al. believed that H₂ could counteract the phosphorylation of IκB and NF-κB, the nuclear translocation of NF-κB p65 protein, and reduce the transcriptional activity of NF-κB.[70] Yang et al. suggested that H₂ could inhibit the activation of NF-κB/NLRP3 pathway, and had a certain therapeutic effect in some diseases.[71] Our study suggested that H₂ entering CECs protected the cells by inhibiting the activation of the NF-κB/NLRP3 pathway under MNU, reducing the nuclear translocation of NF-κB p65, and delaying the process of apoptosis.

Existing evidence shows that p53 is a protein involved in the regulation of a variety of signaling pathways and a threshold regulator of cell homeostasis.[72,73] Under low to moderate oxidative stress, p53 increases the time of cell repair by means of cell cycle arrest. When the intensity and duration of stress continue to increase, p53 activates DNA fragments to induce apoptosis, thus preventing abnormal cell proliferation.[74] The difference in the degree of oxidative stress is the reason for the different effects of p53. P53 protein can promote the increase of p21 expression, thereby inhibiting the cell cycle. Cells cultured in vitro can be called senescence when they lose their proliferative potential (PP), and the expression of p21 can prove the loss of PP, which is irreversible.[74]

The mammalian forkhead box class O (FOXO) transcription factor subfamily includes several highly conserved FOXO proteins, and FoxO3a is one of them.[75] FOXO3a transcription factor is a key regulator of cell metabolism, proliferation, survival, cycle regulation, and apoptosis.[76,77] After stimulation, FOXO3a enters the DNA binding site and is activated for transcriptional activity. Transcription of FOXO target genes is achieved when the nuclear translocation of FOXO3a exceeds a certain threshold.[78] At present, the interaction between FOXO3a and p53 has been widely recognized.[79] We speculate that MNU, as a chemical reagent acting on DNA, may be related to cell senescence in addition to cell apoptosis. The results showed that MNU was associated with increased expressions of FoxO3a, p53, and p21 in CECs, and the entry of FoxO3a into the nuclear binding site. Activation of FoxO3a /p53/ p21 pathway led to pro-apoptotic effect and the effect on the physiological function of CECs, which may be one of the mechanisms of damage of low concentration MNU. Our data suggested that H₂ intervention in CECs could effectively inhibit nuclear translocation of FOXO3a and reduce the expression of FOXO3a, p53, and p21. The mechanism remains to be further studied.

As a convenient and safe form of H₂, the antioxidant properties of HRS can be utilized in a variety of forms, including oral, intraperitoneal, or intravenous injection. It can be presented as local drip, anterior chamber irrigation, or intravitreal injection in ophthalmology, which is safer, more portable, and more effective than inhalation alone.[6,18,20,21,27,46] H₂ can be dissolved in water at a maximum of 1.6 ppm (0.8 mmoL/L) at normal atmospheric pressure and room temperature. It should be used fresh when stored in glass or plastic bottles to prevent H₂ escaping. In our study, the mass ratios of H₂ measured immediately before use were all above 1.2 ppm, which was considered to be sufficient for biological effects internationally.[80,81] The ocular surface irrigation method we used is simple and effective, providing a good reference for clinical use. However, the drawbacks of this method may be that it takes a long time and the hydrogen-rich water is not easy to preserve.

There are two obstacles to the application of H₂, including low reaction rate and short residence time in vivo. Therefore, how to make the safe, simple, and convenient health care products and clinical drugs made by H₂ that could be more widely used may be the direction that many doctors and practitioners of pharmaceutical enterprises should strive for.[18] Other problems puzzling scientific researchers and clinicians are as follows: (1) hydrogen has entered the hot area of therapeutic research in recent years. There are so many roles and biochemical pathways of H₂, and it is difficult to eliminate and utilize the crosstalk among them. (2) Clinical studies, especially large-scale, prospective clinical studies, related to the application of H₂, are urgently needed to optimize the dose, timing and administration method of H₂.

Corneal endothelium decompensation is a serious eye disease that greatly affects the vision of patients. In this study, H$_2$ was used to intervene in the animal models and cell models of corneal endothelial injury induced by MNU. It was confirmed that H$_2$ could effectively and safely reverse the pro-apoptotic effect of MNU on CECs. To our knowledges, the results is the first to be obtained in the laboratory. Furthermore, the anti-apoptotic effect of H$_2$ on CECs was related to antioxidant, the NF-κB/NLRP3 pathway, and the FOXO3a/p53/p21 pathway. Our work lays the groundwork for clinical trials of H$_2$. We speculate that topical application of H$_2$ could protect CECs against corneal injury factors, reduce the damage of corneal endothelium caused by surgeries or toxic substances, reduce the incidence and severity of corneal endothelial disorders, and maintain corneal transparency.

Acknowledgments

Disclosure: **R. Li,** None; **Y. Qu,** None; **X. Li,** None; **Y. Tao,** None; **Q. Yang,** None; **J. Wang,** None; **Y. Diao,** None; **Q. Li,** None; **Y. Fang,** None; **Y. Huang,** None; **L. Wang,** None

References

1. DelMonte DW, Kim T. Anatomy and physiology of the cornea. *J Cataract Refract Surg*. 2011;37:588–598.
2. Bahn CF, Glassman RM, MacCallum DK, et al. Postnatal development of corneal endothelium. *Invest Ophthalmol Vis Sci*. 1986;27:44–51.
3. Joyce NC, Meklir B, Joyce SJ, Zieske JD. Cell cycle protein expression and proliferative status in human corneal cells. *Invest Ophthalmol Vis Sci*. 1996;37:645–655.
4. Gupta K, Deng SX. Corneal endothelial decompensation. *Klin Monatsbl Augenheilkd*. 2020;237:745–753.
5. Matthaei M, Hribek A, Clahsen T, Bachmann B, Cursiefen C, Jun AS. Fuchs endothelial corneal dystrophy: clinical, genetic, pathophysiologic, and therapeutic aspects. *Annu Rev Vis Sci*. 2019;5:151–175.
6. Igarashi T, Ohsawa I, Kobayashi M, et al. Hydrogen prevents corneal endothelial damage in phacoemulsification cataract surgery. *Sci Rep*. 2016;6:31190.
7. America EBAO. Eye Bank Association of America: (2016). Eye Banking Statistical Report [Internet]. Available from: http://restoresight.org/wpcontent/uploads/2017/04/2016_Statistical_Report-Final-040717.pdf.
8. Tan DT, Dart JK, Holland EJ, Kinoshita S. Corneal transplantation. *Lancet*. 2012;379:1749–1761.
9. Gain P, Jullienne R, He Z, et al. Global survey of corneal transplantation and eye banking. *JAMA Ophthalmol*. 2016;134:167–173.
10. Hatou S, Shimmura S. Review: corneal endothelial cell derivation methods from ES/iPS cells. *Inflamm Regen*. 2019;39:19.
11. Qu Y, Li R, Li X, et al. Development of animal models for lens and corneal diseases using N-Methyl-N-nitrosourea. *Invest Ophthalmol Vis Sci*. 2020;61:38.
12. Lijinsky W. Carcinogenicity and mutagenicity of N-nitroso compounds. *Mol Toxicol*. 1987;1:107–119.
13. Faustino-Rocha AI, Ferreira R, Oliveira PA, Gama A, Ginja M. N-Methyl-N-nitrosourea as a mammary carcinogenic agent. *Tumour Biol*. 2015;36:9095–9117.
14. Meira LB, Moroski-Erkul CA, Green SL, et al. Aag-initiated base excision repair drives alkylation-induced retinal degeneration in mice. *PNAS*. 2009;106:888–893.
15. Xiong Y, Ji HP, Song WT, et al. N-methyl-N-nitrosourea induces retinal degeneration in the rat via the inhibition of NF-kappaB activation. *Cell Biochem Funct*. 2016;34:588–596.
16. Tao Y, Cai L, Zhou D, et al. CoPP-induced-induced HO-1 overexpression alleviates photoreceptor degeneration with rapid dynamics: a therapeutic molecular against retinopathy. *Invest Ophthalmol Vis Sci*. 2019;60:5080–5094.
17. Hayakawa R, Komoike K, Kawakami H, et al. Ultrastructural changes in the choriocapillaris of N-methyl-N-nitrosourea-induced retinal degeneration in C57BL/6 mice. *Med Mol Morphol*. 2020;53:198–209.
18. Ge L, Yang M, Yang NN, Yin XX, Song WG. Molecular hydrogen: a preventive and therapeutic medical gas for various diseases. *Oncotarget*. 2017;8:102653–102673.
19. Ohsawa I, Ishikawa M, Takahashi K, et al. Hydrogen acts as a therapeutic antioxidant by selectively reducing cytotoxic oxygen radicals. *Nat Med*. 2007;13:688–694.
20. Tao Y, Geng L, Xu WW, Qin LM, Peng GH, Huang YF. The potential utilizations of hydrogen as a promising therapeutic strategy against ocular diseases. *Ther Clin Risk Manage*. 2016;12:799–806.
21. Zou R, Wang MH, Chen Y, et al. Hydrogen-rich saline attenuates acute lung injury induced by limb ischemia/reperfusion via down-regulating chemerin and NLRP3 in rats. *Shock (Augusta, GA)*. 2019;52:134–141.
22. Qian L, Wu Z, Cen J, Pasca S, Tomuleasa C. Medical application of hydrogen in hematological diseases. *Oxid Med Cell Longev*. 2019;2019:3917393.
23. Slezak J, Kura B, LeBaron TW, Singal PK, Buday J, Barancik M. Oxidative stress and pathways of molecular hydrogen effects in medicine. *Curr Pharm Des*. 2021;27(5):610–625.
24. Wu D, Liang M, Dang H, Fang F, Xu F, Liu C. Hydrogen protects against hyperoxia-induced apoptosis in type II alveolar epithelial cells via activation of PI3K/Akt/Foxo3a signaling pathway. *Biochem Biophys Res Commun*. 2018;495:1620–1627.
25. Cejka C, Kossl J, Hermankova B, Holan V, Cejkova J. Molecular hydrogen effectively heals alkali-injured cornea via suppression of oxidative stress. *Oxid Med Cell Longev*. 2017;2017:8906027.
26. Zhang W, Yu F, Yan C, et al. PTEN inhibition accelerates corneal endothelial wound healing through increased endothelial cell division and migration. *Invest Ophthalmol Vis Sci*. 2020;61:19.
27. Yan WM, Chen T, Wang XC, et al. The reason for the amelioration of N-methyl-N-nitrosourea-induced retinitis pigmentosa in rats by hydrogen-rich saline. *Int J Ophthalmol*. 2017;10:1495–1503.
28. Rosch S, Werner C, Muller F, Walter P. Photoreceptor degeneration by intravitreal injection of N-methyl-N-nitrosourea (MNU) in rabbits: a pilot study. *Graefes Arch Clin Exp Ophthalmol*. 2017;255:317–331.
29. Okumura N, Koizumi N. Regeneration of the corneal endothelium. *Curr Eye Res*. 2020;45:303–312.
30. Patel SV. Graft survival and endothelial outcomes in the new era of endothelial keratoplasty. *Exp Eye Res*. 2012;95:40–47.
31. Van Horn DL, Sendele DD, Seideman S, Buco PJ. Regenerative capacity of the corneal endothelium in rabbit and cat. *Invest Ophthalmol Vis Sci*. 1977;16:597–613.
32. Van den Bogerd B, Zakaria N, Adam B, Matthyssen S, Koppen C, ND S. Corneal endothelial cells over the past

decade: are we missing the mark(er)? *Transl Vis Sci Technol.* 2019;8:13.

33. Bonanno JA. Molecular mechanisms underlying the corneal endothelial pump. *Exp Eye Res.* 2012;95:2–7.

34. Redza-Dutordoir M, DA Averill-Bates. Activation of apoptosis signalling pathways by reactive oxygen species. *Biochim Biophys Acta.* 2016;1863:2977–2992.

35. Fulda S, Gorman AM, Hori O, Samali A. Cellular stress responses: cell survival and cell death. *Int J Cell Biol.* 2010;2010:214074.

36. Waugh DT. The contribution of fluoride to the pathogenesis of eye diseases: molecular mechanisms and implications for public health. *Int J Environ Res Public Health.* 2019;16(5):856.

37. Sun X, Tang Y, Jiang C, et al. Oxidative stress, NF-κB signaling, NLRP3 inflammasome, and caspase apoptotic pathways are activated in mammary gland of ketotic Holstein cows. *J Dairy Sci.* 2021;104(1):849–861.

38. Huang Y, Ma T, Ye Z, et al. Carbon monoxide (CO) inhibits hydrogen peroxide (H(2)O(2))-induced oxidative stress and the activation of NF-κB signaling in lens epithelial cells. *Exp Eye Res.* 2018;166:29–39.

39. MS D'Arcy. Cell death: a review of the major forms of apoptosis, necrosis and autophagy. *Cell Biol Int.* 2019;43:582–592.

40. Rajakumar T, Pugalendhi P, Jayaganesh R, Ananthakrishnan D, Gunasekaran K. Effect of allyl isothiocyanate on NF-κB signaling in 7,12-dimethylbenz(a)anthracene and N-methyl-N-nitrosourea-induced mammary carcinogenesis. *Breast Cancer.* 2018;25:50–59.

41. Cano Sanchez M, Lancel S, Boulanger E, Neviere R. Targeting oxidative stress and mitochondrial dysfunction in the treatment of impaired wound healing: a systematic review. *Antioxidants (Basel, Switzerland).* 2018;7(8):98.

42. Wang D, Li Y, Wang Z, Sun GY, Zhang QH. Nimodipine rescues N-methyl-N-nitrosourea-induced retinal degeneration in rats. *Pharmacognosy Magazine.* 2013;9:149–154.

43. Cejka C, Kossl J, Hermankova B, et al. Therapeutic effect of molecular hydrogen in corneal UVB-induced oxidative stress and corneal photodamage. *Sci Rep.* 2017;7:18017.

44. Ohta S. Direct targets and subsequent pathways for molecular hydrogen to exert multiple functions: Focusing on interventions in radical reactions. *Curr Pharm Des.* 2021;27(5):595–609.

45. Igarashi T, Ohsawa I, Kobayashi M, et al. Effects of hydrogen in prevention of corneal endothelial damage during phacoemulsification: a prospective randomized clinical trial. *Am J Ophthalmol.* 2019;207:10–17.

46. Kubota M, Shimmura S, Kubota S, et al. Hydrogen and N-acetyl-L-cysteine rescue oxidative stress-induced angiogenesis in a mouse corneal alkali-burn model. *Invest Ophthalmol Vis Sci.* 2011;52:427–433.

47. Gao L, Jiang D, Geng J, Dong R, Dai H. Hydrogen inhalation attenuated bleomycin-induced pulmonary fibrosis by inhibiting transforming growth factor-β1 and relevant oxidative stress and epithelial-to-mesenchymal transition. *Exp Physiol.* 2019;104:1942–1951.

48. Nandi A, Yan LJ, Jana CK, Das N. Role of catalase in oxidative stress- and age-associated degenerative diseases. *Oxid Med Cell Longev.* 2019;2019:9613090.

49. Yazdani M. Concerns in the application of fluorescent probes DCDHF-DA, DHR 123 and DHE to measure reactive oxygen species in vitro. *Toxicol In Vitro.* 2015;30:578–582.

50. Sun SC. The non-canonical NF-κB pathway in immunity and inflammation. *Nat Rev Immunol.* 2017;17:545–558.

51. Afonina IS, Zhong Z, Karin M, Beyaert R. Limiting inflammation-the negative regulation of NF-κB and the NLRP3 inflammasome. *Nat Immunol.* 2017;18:861–869.

52. Xiong Y, Ji HP, Song WT, et al. N-methyl-N-nitrosourea induces retinal degeneration in the rat via the inhibition of NF-κB activation. *Cell Biochem Funct.* 2016;34:588–596.

53. Taniguchi K, Karin M. NF-κB, inflammation, immunity and cancer: coming of age. *Nat Rev Immunol.* 2018;18:309–324.

54. Mussbacher M, Salzmann M, Brostjan C, et al. Cell type-specific roles of NF-κB linking inflammation and thrombosis. *Front Immunol.* 2019;10:85.

55. Saha A, Hammond CE, Trojanowska M, Smolka AJ. Helicobacter pylori-induced H,K-ATPase alpha-subunit gene repression is mediated by NF-kappaB p50 homodimer promoter binding. *Am J Physiol Gastrointest Liver Physiol.* 2008;294:G795–G807.

56. Shao A, Wu H, Hong Y, et al. Hydrogen-rich saline attenuated subarachnoid hemorrhage-induced early brain injury in rats by suppressing inflammatory response: possible involvement of NF-kappaB pathway and NLRP3 inflammasome. *Mol Neurobiol.* 2016;53:3462–3476.

57. Zou Y, Cui B, Liang P, Tian X, Ma Y, Zhao S. Inhibition of NLRP3 protects human lens epithelial cells against oxidative stress-induced apoptosis by NF-κB signaling. *Ophthalmic Res.* 2020;63:174–181.

58. Kelley N, Jeltema D, Duan Y, He Y. The NLRP3 inflammasome: an overview of mechanisms of activation and regulation. *Int J Mol Sci.* 2019;20(13):3328.

59. Moloudizargari M, Moradkhani F, Asghari N, et al. NLRP inflammasome as a key role player in the pathogenesis of environmental toxicants. *Life Sci.* 2019;231:116585.

60. Shimizu H, Sakimoto T, Yamagami S. Pro-inflammatory role of NLRP3 inflammasome in experimental sterile corneal inflammation. *Sci Rep.* 2019;9:9596.

61. Mekni N, De Rosa M, Cipollina C, et al. In silico insights towards the identification of NLRP3 druggable hot spots. *Int J Mol Sci.* 2019;20(20):4974.

62. Schroder K, Tschopp J. The inflammasomes. *Cell.* 2010;140:821–832.

63. Franchi L, Eigenbrod T, Muñoz-Planillo R, Nuñez G. The inflammasome: a caspase-1-activation platform that regulates immune responses and disease pathogenesis. *Nat Immunol.* 2009;10:241–247.

64. Keller M, Rüegg A, Werner S, Beer HD. Active caspase-1 is a regulator of unconventional protein secretion. *Cell.* 2008;132:818–831.

65. Wang Y, Shi P, Chen Q, et al. Mitochondrial ROS promote macrophage pyroptosis by inducing GSDMD oxidation. *J Mol Cell Biol.* 2019;11:1069–1082.

66. Zheng Q, Ren Y, Reinach PS, et al. Reactive oxygen species activated NLRP3 inflammasomes prime environment-induced murine dry eye. *Exp Eye Res.* 2014;125:1–8.

67. Oh JY, Ko JH, Ryu JS, Lee HJ, Kim MK, Wee WR. Transcription profiling of NOD-like receptors in the human cornea with disease. *Ocul Immunol Inflamm.* 2017;25:364–369.

68. Chen H, Zhou C, Xie K, Meng X, Wang Y, Yu Y. Hydrogen-rich saline alleviated the hyperpathia and microglia activation via autophagy mediated inflammasome inactivation in neuropathic pain rats. *Neuroscience.* 2019;421:17–30.

69. Chen H, Mao X, Meng X, et al. Hydrogen alleviates mitochondrial dysfunction and organ damage via autophagy–mediated NLRP3 inflammasome inactivation in sepsis. *Int J Mol Med.* 2019;44:1309–1324.

70. Wu G, Pan L, Sun J, Chen G, Wang S. Hydrogen gas protects against ovariectomy-induced osteoporosis by inhibiting NF-κB activation. *Menopause (New York, NY).* 2019;26:785–792.

71. Yang L, Guo Y, Fan X, et al. Amelioration of coagulation disorders and inflammation by hydrogen-rich solution reduces intestinal ischemia/reperfusion injury in rats through NF-κB/NLRP3 pathway. *Mediators Inflamm.* 2020;2020:4359305.

72. Petrova NV, Velichko AK, Razin SV, Kantidze OL. Small molecule compounds that induce cellular senescence. *Aging Cell*. 2016;15:999–1017.

73. Yaghoobi MM, Sheikoleslami M, Ebrahimi M. Effects of hydrogen peroxide, doxorubicin and ultraviolet irradiation on senescence of human dental pulp stem cells. *Arch Oral Biol*. 2020;117:104819.

74. Beyfuss K, Hood DA. A systematic review of p53 regulation of oxidative stress in skeletal muscle. *Redox Rep*. 2018;23:100–117.

75. Monsalve M, Olmos Y. The complex biology of FOXO. *Curr Drug Targets*. 2011;12:1322–1350.

76. Nguyen LT, Lee YH, Sharma AR, et al. Quercetin induces apoptosis and cell cycle arrest in triple-negative breast cancer cells through modulation of Foxo3a activity. *Korean J Physiol Pharmacol*. 2017;21:205–213.

77. Eijkelenboom A, Burgering BM. FOXOs: signalling integrators for homeostasis maintenance. *Nat Rev Mol Cell Biol*. 2013;14:83–97.

78. Pronsato L, Milanesi L, Vasconsuelo A, La Colla A. Testosterone modulates FoxO3a and p53-related genes to protect C2C12 skeletal muscle cells against apoptosis. *Steroids*. 2017;124:35–45.

79. Wang F, Marshall CB, Yamamoto K, et al. Biochemical and structural characterization of an intramolecular interaction in FOXO3a and its binding with p53. *J Mol Biol*. 2008;384:590–603.

80. Ohta S. Recent progress toward hydrogen medicine: potential of molecular hydrogen for preventive and therapeutic applications. *Curr Pharm Des*. 2011;17:2241–2252.

81. George JF, Agarwal A. Hydrogen: another gas with therapeutic potential. *Kidney Int*. 2010;77:85–87.